공학박사 학위논문

OPTICAL ACTIVATION OF CULTURED NEURONS USING ULTRA-SHORT PULSE

펨토초 빛을 이용한 신경세포 자극방법

2015년 8월

서울대학교 대학원

협동과정 뇌과학전공

장 재 명

OPTICAL ACTIVATION OF CULTURED NEURONS USING ULTRA-SHORT PULSE

지도 교수 전 누 리

이 논문을 공학박사 학위논문으로 제출함

2015 년 6 월

서울대학교 대학원

협동과정 뇌과학 전공

장 재 명

장재명의 공학박사 학위논문을 인준함

2015 년 7 월

위 원 장 김 성 준 (인)

부위원장 전 누 리 (인)

위 원 오 우 택 (인)

위 원 정 웅 규 (인)

위 원 최 영 식 (인)

Abstract

Optical activation of cultured neurons using ultra-short pulse laser

Jang, Jae Myung
Interdisciplinary program in neuroscience
The Graduate School
Seoul National University

The paradigm of experimental models in modern neuroscience and neural engineering has been rapidly evolving from 2D to 3D environments. A variety of techniques have emerged as important tools for controlling action potential firing of a single neuron in 3D environments. Here, we report that a focused femtosecond light activates an unmodified neuron in a 3D environment, producing repetitive action potentials without insertion of any external materials. To further characterize this method, a new microfluidic system was developed to optically stimulate a neuron and electrically record its signals for a long duration. This was combined with the microfluidic technique and electrode measurement under the microscope. This approach allowed precise and rapid stimulation of a single neuron at

multiple points, and systematic analyses of neural and axonal responses using a spike sorting technique. We assessed the property, efficiency, and safety of this optical stimulation using the focused femtosecond light. We also demonstrated that the femtosecond light stimulated a neuron successfully in 3D environments. Furthermore, the studies on the underlying mechanism indicated that the neural response to femtosecond light was caused by intracellular calcium elevation from the internal calcium store through supra-threshold excitation of the soma.

Although several factors remain to be determined regarding femtosecond light irradiation, we expect that this technique will avoid many of the problems inherent to electrodes, such as invasiveness and lack of specificity, and thus, could aid in scientific discoveries and in engineering experimental approaches. Furthermore, the femtosecond light coupled with an appropriate optical probe can be employed for in vivo neural stimulation. This may lead to new therapeutic approaches with rapid optical regulation of excitation and inhibition without genetic modification and external interruption of the cellular function.

Keywords: Femtosecond light, optical stimulation, neuron, microelectrode-arrays, intracellular calcium influx

Student Number: 2011-30132

Contents

List of Tables

List of Figures

Chapter 1. Introduction

1.1. Motivation

The introduction of electrophysiological tools marked the beginning of a new era in modern neuroscience. The idea that the nervous system works electrically has been understood since Galvani's experiments revealed that electricity existed in animals [1]. However, the experimental instruments to easily and precisely manipulate neural activity in the nervous system, as well as to measure electricity, did not exist before the invention of electrodes. The electrodes that Helmholtz used to discover nerve conduction speed have been widely popularized in the search to acquire knowledge about the brain and nervous system. Their application in research ranges from studying an ion channel's properties *in vitro*, to probing neural circuitries, to treating neurological disorders and restoring sensory function *in vivo*.

A meaningful advance in neural techniques was the development of the microelectrode for recording the activity of a single neuron in the brain. The first extracellular recording with a microelectrode was performed in the hippocampus [2]. The role of individual neurons in the motor cortex or visual cortex in response to motor control or visual stimuli, respectively, was also characterized by using the electrical technique to record single neuron activity [3, 4]. Intracellular recording of the activity of a single neuron in the brain was pioneered during work on cortical neurons [5-8]. Following

comprehensive intracellular recording from the cortex, recording the activity of a single hippocampal pyramidal cell was achieved [9]. Subsequently, the development of recording technique with double electrode [10], tetrodes [11], and microelectrode-arrays (MEAs) [12] allowed simultaneous recording of a large number of neurons by separating each individual neuron's activity.

Contrary to the development of these recording techniques, the growth of neural stimulation with microelectrodes was stagnant for a long time. Methods to stimulate a neuron electrically were developed and primarily divided into two categories: current-controlled stimulation and voltage-controlled stimulation. In current-controlled stimulation, the electrons flow easily under the user's control and the electric field near the microelectrodes is precisely calculated. However, high currents cause high charge injection or high charge densities that are enough to damage a cell. The voltage-controlled stimulation also has a similar constraint because of the electrolysis that occurs and directly damages the microelectrodes when the electrode voltage exceeds about 1 V. Moreover, both of the electrical stimulation methods have a limited pulse duration time. It is impossible to record neural signals simultaneously to the electrical stimulation since they convert the stimulus into artifacts. Therefore, electrical stimulation is applied for as short a time as possible.

Furthermore, electrical stimulation should always utilize more than two microelectrodes, cathodes and anodes. Electrical stimulation generates electrical fields that are large enough to cover multiple neurons in the vicinity of the microelectrodes. Even after closing the distance between two

microelectrodes using micromanipulators, the flow of electrons is not restricted to the localized single neuron. Membrane potential and ion concentrations are not homogeneous and an ionic aqueous solution creates additional impedance around the neuron, causing the electrons delivered from the microelectrode to travel along a path with lower impedance. Another approach for single neuron stimulation is to seal a pipette containing a microelectrode onto the neuron's membrane, thus providing a connection to the intracellular space of the neuron. However, the cytosolic materials of the neuron's interior are replaced with the high-potassium content of the electrode. Its suction often ruptures the cellular membrane, inducing the cell's death. Because the volume of a glass pipette is larger than the volume of a neuron, it is difficult to move its position and to stimulate multiple neurons simultaneously. Moreover, the major drawback is that it is very laborious and time-consuming, and dependent on personal skillful experience.

Mechanical stimulation has also been suggested as one of the alternatives to electrical stimulation. Previous studies used experimental models to study the cellular response to mechanical stimuli. Insertion of a small glass micropipette [13], an injection of a 4% agar solution into trigeminal nerve roots [14], a micro-vascular clip for cervical nerve roots [15], or implantation of stainless steel rods into dorsal root ganglion cells [16], were used as *in vivo* models of mechanical compression. Similarly, several techniques apply force to the *in vitro* cells. An atomic force microscope also puts pressure on a cell through a fine tip [17-19].

Mechanical stimulation of an astrocyte induced a wave of an increased number of intracellular calcium ions [13]. However, this mechanical stimulation is also harmful to a neuron. It is necessary to inject an invasive medium to make contact with the cellular membrane, similar to the insertion of a microelectrode. Therefore, non-invasive neural stimulation of a single neuron in brain tissue or three-dimensional (3D) environments with either electrical or mechanical methods is impossible. Specifically, culturing cells in a 3D microenvironment has been used in mainstream research over the last several decades. The 3D *in vitro* models have been developed with various technologies such as beads, silk, electro-spinning, and silicon wafers, including an explant of brain tissue, organotypic culture from thin slices, and cell-based constructs [20-23]. Significant advances in engineering hydrogels as a scaffold material resulted in three-dimensional cell-based models for a variety of tissues [24-27]. Two-dimensional (2D) cell cultures do not adequately mimic the features of living organs. They fail to reconstitute cell behavior, cell-to-cell interaction, as well as cellular and mechanical microenvironments. The 3D *in vitro* models were able to maintain several advantages of *in vitro* cultures as well as to recapitulate many critical aspects of native tissue as a result of the hydrogel's high water content, biocompatibility, and chemical/physical properties. In this background, the importance of neural stimulation in a 3D culture was emphasized. However, both the brain tissue and the 3D cell culture have depth on the z-axis. The conventional neural stimulation method is indispensable to penetrating microelectrodes, destructing brain tissue and 3D culture samples.

1.2. Optical stimulation with photochemical molecules

The first breakthrough to meet the demand for methods enabling non-invasive neural stimulation in brain tissue or 3D cultures was the introduction of exterior materials to manipulate neural activity [28]. As is well known, a neuron delivers information using chemical molecules such as neurotransmitters and several ions, with the exception of electrons. Therefore, chemical excitation by regulation of the concentration of neurotransmitters (or ions) or by controlling the ion channels associated in action potentials was one of the most common ways to stimulate a neuron. The handling of a polymer coated with a chemical structure that resembled neurotransmitters was also suggested as a new neural stimulation technique [29]. However, all of molecules in aqueous solution diffuse as a result of the random motion from their kinetic energy. Therefore, chemical stimulation has the fundamental limitation of low temporal and spatial resolution in 3D as well as 2D environments.

To solve this problem, the photochemical molecules whose structure was changed in response to light were synthesized. Most of developed tools are placed in one of three categories: caged neurotransmitters, natural photosensitive proteins, and small molecule photo-switches. Caged neurotransmitters decomposed by light release neurotransmitters, binding to their receptors for influencing intracellular signal transduction. Genetic insertion of natural photosensitive proteins such as ChR2 from the algae Chlamydomonas into mammalian neurons was sufficient to allow neuronal

firing. Moreover, photo-switches were synthesized to link a photo-isomerizable molecule to a normal ion channel or a receptor. At present, these methods enable users to manipulate neural activity with temporal and spatial accuracy in 3D environments. The time and the area of the photoreaction can be controlled by the exposure time and the intensity of the light. Furthermore, the application of two-photon absorption to photochemical techniques can overcome the conventional technical limitations [30]. Two-photon absorption is explained as a process in which an atom absorbs two or more successive photons to induce a molecular transition to an excited electronic state. Two-photon absorption occurs simultaneously through a virtual state, to where the absorption of the first photon is thought to excite the molecule, with a very short lifetime on the order of 10^{-15} s. The absorption of the second photon during this lifetime is necessary for two-photon absorption. And two-photon absorption takes places when two photons arrive in a specific area within an appropriate time so that they may be absorbed together. Two-photon absorption is quantified as the product of two factors, areas and time, in units of Goeppert-Meyer (GM), where 1 GM is 10^{-50} cm^4s/photon. Therefore, two-photon stimulation with a spatial resolution of 1 μm^2 around the focal point afforded efficient control over the individual stimulation of the dendritic (or axonal) trees of a neuron. Combining the advantages of two-photon absorption and photochemical methods has revolutionized the capacity to understand neural circuits and their excitatory transmission in neurons [31-35]. Controlled and localized activation of synapses revealed how an individual neuron worked,

and how it encoded and decoded information.

However, the addition of exterior materials can pose other risks to a neuron. It may result in an imbalance of ion concentrations beyond homeostasis for living organisms, thus changing osmotic concentrations. The artificial elevation of neurotransmitter concentrations around a neuron can induce excitotoxicity when receptor over-activation results in high levels of intracellular calcium. A calcium influx induced by glutamate activates enzymes such as phospholipase, endonuclease, or protease, which damages cytoskeletons, membranes, and DNA, respectively [36-39]. Genetic insertion also has several challenges that remain, such as extent, efficiency, and tolerance. It also has fundamental constraints for broad application in non-human primate science, including neural prosthetics research [40-42]. Specifically, the photochemical materials have been reported to express in specific types of neurons [43]. Therefore, these reasons still prevent the addition of the exterior materials as a substitute for the electrical stimulation with microelectrodes in 3D environments, blocking immediate application to a widespread human study.

1.3. Non-invasive neural stimulation using Focused Ultrasound and Magnetic Fields

Focused ultrasound has been introduced as a new modality to satisfy the demands of non-invasive and safe stimulation in 3D environments [44-47]. The method uses ultrasound transducers to yield highly localized acoustic

energy into a focused point. The longitude waves with frequencies of more than 20 kHz propagate through brain tissue and fluids. The transducer configuration and fundamental acoustic frequency determine spatial resolution up to a few millimeters. Lower acoustic frequencies (<1 mHz) are the minimum acoustic intensity required to stimulate a neuron without hampering, providing superior penetration depth that is enough to stimulate brain tissue through an intact skull or in a 3D neuron culture [48-50].

The first trials to stimulate a neuron with the focused ultrasound showed that it could inhibit the spontaneous activity in the brain of animals [51-53]. However, high intensity focused ultrasound (8~4500 W/cm2 at 0.48~3 MHz) was reported to ablate tissue in localized areas in the brain. In contrast, the technique of low intensity focused ultrasound pulsation having less than 100 W/cm^2 at less than 1 MHz has been proposed. Subsequently, it has been reported to modify the electrically evoked spikes in cultured hippocampal neurons for 40~50 ms [54]. Recently, the feasibility of neural stimulation with a variety of pulsing schemes or continuous waves has been studied [55]. However, this external stimulus still lacks spatial specificity of up to a few millimeters.

Magnetic stimulation is also emerging as a new neural stimulation tool for non-invasive methods with adequate penetration depth, similar to the focused ultrasound methods. It consists of two components, the first being a current carrying coil that produces a pulsed, high strength field, and the second being a charge-discharge system, including switching circuitry and a controller. A coil of wire produces magnetic flux lines, perpendicular to the

plane of the coil. An electrical field is induced due to the inductive nature of magnetic fields, which causes the electrical charge's flow in the medium [56-62]. Due to these properties, the design of a wire coil is critical to determine the induced current distribution and the site of stimulation. Commonly used coils were designed with single circular loop or two circular coils in parallel similar to a butterfly shape. In addition, the switching system of repetitive capacitive charging is important in magnetic stimulation. It is able to increase the induced current decay time and eliminate reverse currents. Therefore, it gives the circuits a series of pulses. Recent development of magnetic field generation allows upward of 100 Hz stimulation frequencies. It was firstly shown that the external magnetic stimulation was able to activate neurons in the targeted motor cortex through the intact human scalp [63]. It is now commonly used to excite or inhibit neurons in brain tissue, even though there is still uncertainty as to how the magnetic field stimulates neurons. Moreover, merging with other brain-imaging techniques such as EEG, PET, SPECT, or fMRI gives us new opportunities to explore brain function. However, it also has the drawback of poor spatial resolution such that it can only stimulate neurons in the brain for an area less than 2 cm^2.

1.4. Overview

In summary, the current state of research in neural stimulation is lacking in demands for high spatial and temporal resolution to a single neuron in 3D environments. It is additionally crucial to prevent damaging or killing cells. Once damaged, it becomes difficult to reproduce evoking spikes from the targeted neuron.

Here, we demonstrate a novel technique to stimulate a single neuron in 3D environments using light. To evaluate the neural response systematically, we installed the experimental set-up on an inverted microscope. It allows culturing neurons on the microscope for a long time using the customized incubator with a temperature controller and a CO_2 inlet. It was combined with planar microelectrode-arrays (MEAs) and microfluidic device, recording neural signals from soma and axons separately in response to any external stimulus. Spikes were analyzed to detect the action potentials' rate, pattern, and waveform, from the stimulated neuron by spike sorting technique.

Before irradiation of femtosecond light, we stimulated neurons using photolysis of commercial caged glutamate (MNI-caged glutamate) for evaluation of our system before introduction of femtosecond light. The periodic response to the glutamate released by photo-stimulation was measured at both of soma and axons with the help of the microfluidic system. And we found that visible light from a general fluorescent source allowed decomposing from the caged-glutamate known as only the reaction with UV

wavelength. Furthermore, the threshold level was constant over exposure radiant multiplied with pulse duration and light intensity, dependent on the caged glutamate's concentration. The number of evoked spikes in response to photo-stimulation with caged glutamate was quantified for optimizing optical parameters.

And then, the femtosecond light was introduced to a neuron without insertion of the external materials. The femtosecond light evoked repetitive spikes from a single neuron. Its rate was 20~30 Hz regardless of optical parameters – exposure duration, intensity, once the neuron was activated. It waveform, first negative, and then next positive represented that the response to femtosecond light was valid in only the soma. We confirmed the reproducibility and the safety of the technique. Finally, for the safe use of femtosecond light in brain stimulation, we suggested the parameter range to prevent unwanted mechanical or thermal damage to the neuron during and after the exposure.

Furthermore, we suggest the mechanism of femtosecond-induced neural activation. The analysis of repetitive spike in soma and the blocker treatment with the voltage-sensitive ion channels represents that the focused femtosecond light leads supra-excitation with increase of calcium level. The pharmacological studies also reveal that the calcium increased by the femtosecond light comes from intracellular organelle.

Additionally, future investigations will be needed to develop a new tool for *in-vivo* application that allow the femtosecond light to contribute actively to the neural stimulation.

Chapter 2. Methodology

2.1. Neural recording system

The exposure was synchronized with the recording system by a trigger signal on the TTL output of the shutter controller. For the electrophysiological measurements, neurons were plated at a density of 6 × 10^6 cells/mL on a MEAs, which consisted of an 8 × 8 array of planar microelectrodes. The diameter of each electrode was 10 ~ 30 μm and the electrode spacing was 100 ~ 200 μm. For electrophysiological recordings, extracellular action potentials of each culture were recorded using a 64-channel extracellular recording system consisting of a 64-channel pre-amplifier, a 64-channel main amplifier, and a data acquisition board. The data was recorded with a sampling rate of 10 kHz for 5 min. All laser experiments were performed at 22 °C.

2.2. Fabrication of the microfluidic device

The master mold wafer was fabricated using photolithography. Molds for the PDMS pieces were made using standard soft lithography with SU-8 on silicon wafers. To build the microfluidic device, SU-8 2002 (MicroChem, USA) was spin coated onto a wafer at 3500 rpm for 30 s, at the desired height of 3 μm. The SU-8 was soft baked at 95°C for 5 minutes, exposed to

UV light on a Mask aligner for 5 s, and then baked again. Following a hard bake, the second layer was spun on. Culture chambers were made using two layers of SU-8 100 in which the first layer was spun on at 1000 rpm for 30 s and then baked, and then the second layer was directly spun on after the first layer cooled. After the second layer cooled, the SU-8 was exposed for 30 s, and then baked again. Development was performed upside down for 30 minutes.

PDMS culture chambers were open at both ends to facilitate the exchange of the medium and oxygen. PDMS (Sylgard 184, Dow Corning, USA) was poured onto the structured wafers and allowed to redistribute for 1 hour. It was cured at 60–80°C for at least 4 hours. The PDMS cast was cut into pieces to yield the individual chamber and channel devices, which were then cleaned with isopropanol and blown dry with N2 gas. The chip surface was also cleaned with isopropanol and blown dry. The PDMS device was placed onto the array with a pair of tweezers and pushed down.

The microfluidic device for a 3D culture was designed to replace ECM components of the Matrigel with the micro-pillar arrays. The microfluidic device for 3D cultures allows each of the 3 distinct channels to be selectively filled with different cells mixed with hydrogels, or media. The central channels were first filled with Matrigel whilst the remaining channels were occupied with the media. The previous micro-pillar shape was changed from a hexagonal shape to a regular triangle with 100-μm sides at 100-μm intervals in order to avoid air interruption. Liquid Matrigel at 4˚C was loaded into these channels and placed in the micro-pillar arrays.

2.3. Procedure of primary culture

All procedures were performed in accordance with protocols approved by the Seoul National University Institutional Animal Care and Use Committee. Hippocampal neurons were isolated from fetal Sprague-Dawley rats (Samtaco, Korea) of 17–18 days of gestation. Neurons were dissociated by treatment with 0.25 % trypsin-EDTA (Gibco, USA) in Ca^{2+}-free and Mg^{2+}-free Hank's balanced salt solution (Gibco, USA) for 15 min at 37 ◦C. After incubation, the supernatants were removed and Dulbecco's Modified Eagle's medium (Gibco, USA) containing 10% fetal bovine serum was added to stop the trypsin reaction. The supernatants were removed again before the Neurobasal medium containing 2% B27 supplement (Gibco, USA), 0.25% GlutaMax (Gibco, USA), and 1% penicillin-streptomycin (Invitrogen, USA) was added. They were seeded at a density of 6×10^6 cells/mL in a microfluidic device whose base was coated with poly-D-lysine. The dissociated neurons were maintained at 37 ◦C in air containing 5% CO_2 at saturation humidity and cultured for 3 weeks.

For calcium imaging experiments, neurons were loaded for 15~60 minutes at 37 ◦C with the calcium-sensitive fluorescent dye fluo-4/AM (F14201, Life technologies, USA) diluted in the neurobasal media. Additionally, Pluronic F-127 (P-6867, Life technologies, USA) was dissolved in DMSO to make a 20% (w/v) solution. Both solutions were mixed at the same volume, and then incubated at 37 ºC for 30 minutes.

2.4. Image analysis

Cells in the microfluidic device on the planar microelectrode arrays were imaged using fluorescence or phase contrast microscopy. The two modes show the structural information to check the stimulated cells and the functional information of intracellular calcium. Images were taken with fluorescence and phase contrast microscopy, and fluorescence sequences were recorded using Fluo-4 loaded cells. The image sequences were analyzed by ImageJ software (US National Institutes of Health, USA).

2.5. Data analysis

Extracellular recording simultaneously captured a variety of signals at multiple neurons around a single electrode. Discrete-time detection and classification of neural spikes in extracellular recording is a prerequisite for the analysis of a single cell's behavior and the reconstruction of spike trains. In most experimental neural recording, these spikes are usually recorded in the presence of noise. Therefore, the recorded raw data should be filtered to eliminate low-frequency signals such as 60 Hz noise or low-field potentials (LFPs) using a band pass filter. Thus, the spikes were extracted following a comparison with the threshold voltage value computed as 3.5 ~ 5 times the standard deviation noise and the band-pass filtered data.

Once spikes are detected, the waveform of each action potential is extracted from the data. It is common to align spikes on the threshold

crossing found during spike detection [64]. The waveforms extracted from spike trains are different each other. For classifications of the same waveform, it is required to extract distinctive features from the spike shapes.

Therefore, the principal component analysis (PCA) is used to correct the problem. The PCA is mathematically calculated to transform the raw data to a new coordinate system. It projects the aligned spikes onto an orthogonal axis and reduces their dimensions into 2 or 3 components.

Taking a group with the same waveform, we applied a cluster analysis to the results of the PCA analysis. There are many types of clustering analyses, such as hierarchical clustering, K-means clustering, Gaussian distributions based on an expectation-maximization algorithm, and density-based clustering [65]. There is no accurately defined "standard" clustering analysis. The best clustering analysis is chosen, depending on the particular application. Here, we chose a clustering analysis using the mixture of a Kalman filter [66], as it was noted that this method used in conjunction with the PCA showed a high accuracy capability.

2.6. Experimental Set-up

The novel experimental configuration for these experiments comprised a microfluidic device coupled to microelectrode-arrays, an inverted microscope (IX70, Olympus, Japan) with a customized culture chamber (Live cell instruments), a CCD camera (Moticam Pro 205C, Motic, China), a 60-channel extracellular recording system (USB-ME64, multichannel

systems, Germany), and two-kinds of light sources for one- and two-photon stimulation, as shown in Figure 2.1. Whenever any incident light passes the mechanical shutter (SH05, Thorlabs, USA), a trigger signal was delivered to all devices for time synchronization. In the experiment, both 140 fs, 700-nm-center-wavelength pulsed light from an amplified Ti: sapphire laser (Cameleon Ultra, Coherent, USA) and continuous visible light ranging from 300–600 nm LED (SOLA light engine, Lumencor, USA) entered an inverted microscope via a dichroic mirror. They were focused by a 0.7-N.A. 60× objective lens to the center of the cultured neurons inside the microfluidic channel device and were coupled with 1-mm-thick glass planar microelectrode arrays on an inverted microscope. Images were delivered to a CCD camera through a phase contrast microscope. The neural signals were measured at a 10 kHz sampling rate with a 60-channel extracellular recording system. The microfluidic device is designed to separate signals of the axons from the soma and made with polydimethylsiloxane (PDMS). The frequently used process for microfluidic devices is replica molding of PDMS using a master on the wafer, micro-manufactured through epoxy polymer photoresist and SU-8 photolithography, as previously explained. The PDMS microfluidic device is attached to the microelectrode-arrays instantly, and then treated with plasma cleaning for 5 min to make their surface hydrophilic.

The experimental set-up employs a customized chamber (Live Cell Instruments, Korea) supported with a 37°C temperature controller and a humidified 5% CO_2 gas inlet for the prolonged culturing of neurons on the

inverted microscope, shown in Figure 2.2. In addition, a XY-auto stage (Live Cell Instruments, Korea) and a Z-motorized stage (Applied Scientific Instruments, USA) are installed on the microscope. The PDMS device is minimally sized, in order to insert it into the glass ring of microelectrode-arrays. The space between the device and the ring of the microelectrode array is filled with media in order to prevent evaporation, which changes medium osmolality and causes cell death. These properties of the experimental set-up provide reproducibility of optical stimulation out of an incubator, as well as precise position control over where the light is focused for irradiation. Furthermore, the design permits simultaneous monitoring cell morphology in the microfluidic device through the microscope, and measurement of their electrical activity with microelectrode-arrays.

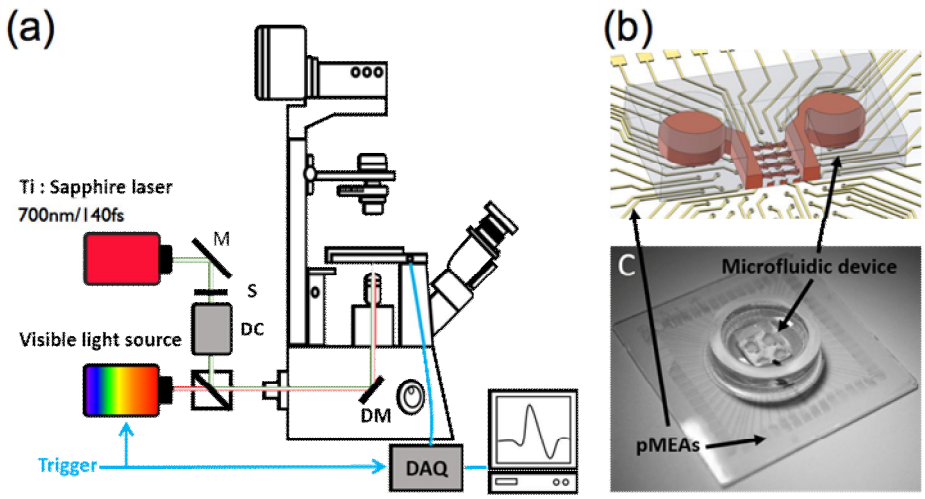

Figure 2.1. Overview of a new microfluidic system for optical stimulation *in vitro* (a) Schematic of the experimental set-up, which shows two kinds of light path through the back port of the inverted microscope as well as a customized incubator on the microscope. The trigger signal having TTL type was used to synchronize the light source with DAQ for neural recording. (b) Integrated device combined with a microfluidic culture platform and a planar MEA. (c) A real image of the integrated device displays that the PDMS microfluidic device is placed in the ring of MEA. M: mirror, S: shutter, DM: dichroic mirror, DC: dispersion compensator, DAQ: data acquisition system, MEA: micro electrode-arrays

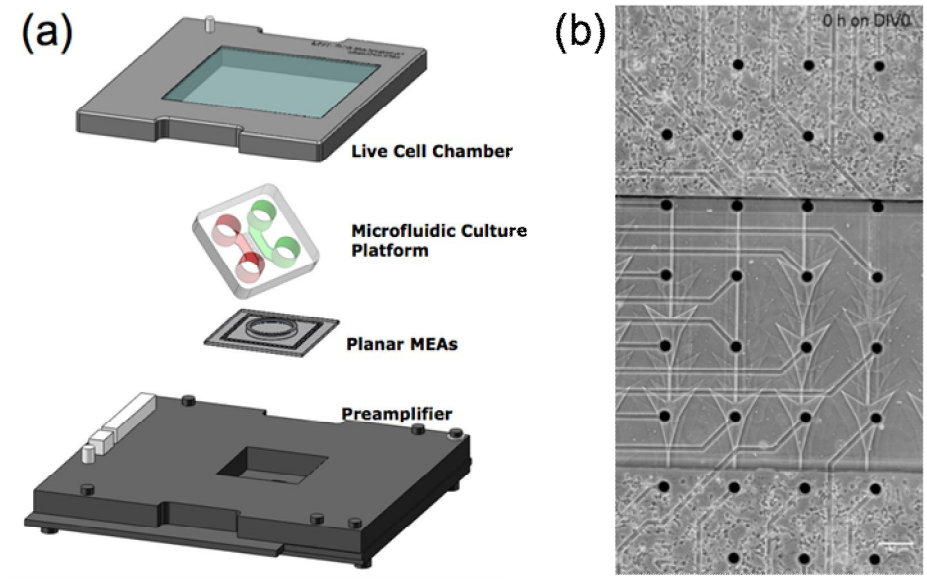

Figure 2.2. Overview of the customized chamber installed on the inverted microscope for long-term culture. (a) Components of Experimental set-up for long-time culture are a live chamber cover, microfluidic culture device, a planar MEAs, and preamplifier. The live cell chamber plays a role to maintain the CO_2 concentration and the bottom plate of the preamplifier supports 37°C temperature of the media in the planar MEAs (b) An example image (DIV0) of neurons cultured in the customized chamber on the microscope for two weeks.

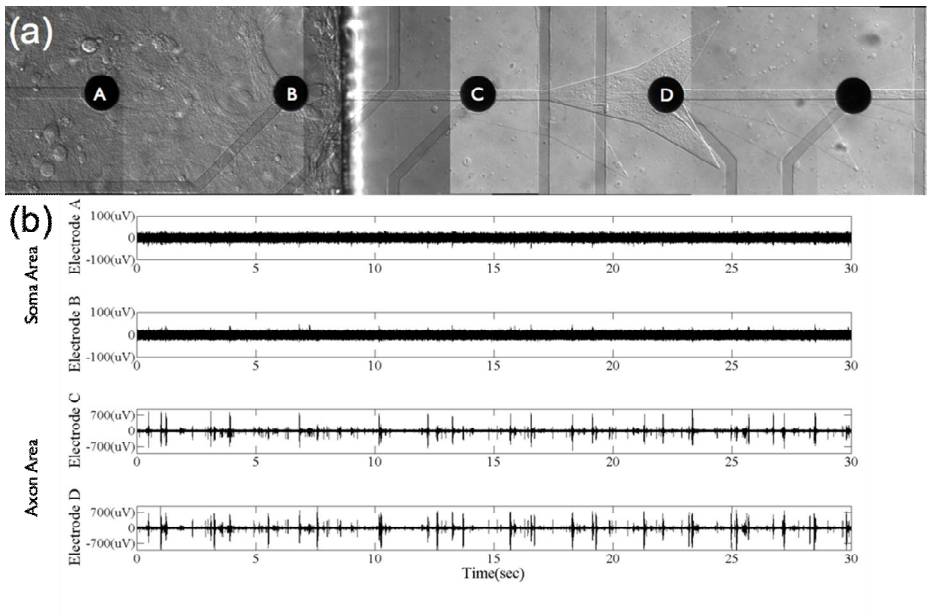

Figure 2.3. Capability of the new microfluidic system dividing into soma and axon. (a) Image of neurons in the microfluidic culture device on microelectrode arrays. The soma (A, B) and the axon (C, D) were cultured separately in the microfluidic system. (b) The soma's and the axon's signals were recorded simultaneously from each region corresponding to A/B and C/D electrode. The amplitude of electrodes around the soma was ±100μV, while that of electrodes that pass through axons was ±700μV.

We continuously acquired images of cultured neurons in a microfluidic device using the Micro-Manager software (US NIH, USA) and their raw neural signals using the MC_Rack software (multichannel systems, Germany) simultaneously on the same computer; the values are plotted in Figure 2.3(b). The images acquired at 13 days *in vitro* showed that upon random plating of neurons in the micro-channels, the axons grew into micro-grooves [67] while the soma was still present in the micro-channels (Figure 2.3(a)). The spontaneous activities of cultured hippocampal neurons on each electrode were measured simultaneously. The average noise level was less than 50 μV peak-to-peak and action potentials were detected using an amplitude threshold. This threshold was set as a multiple of the standard deviation of the background noise The microfluidic device permits imaging of structured networks of approximately 3 μm by 10 μm in cross-section, too small for cell bodies, but open to axonal extension. This makes it possible to divide the two parts into the cell bodies in micro-channels and the axons in micro-grooves, as shown in previous studies. Furthermore, neural signals from the axons were also distinguished from those in the soma, with simultaneous observation of the neuron's morphology. Average signal amplitudes of peak-to-peak voltage exceeding 250 μV are common in the micro-grooves for axons and 20 times greater than those recorded in micro-channels for the soma. The large signal amplitude of the peak-to-peak voltage is caused by the increase of total impedance from 200 kΩ to 1.7 MΩ in the microgrooves. The resistance in the microgroove is proportional to the product of its height (3 μm) and width (10 μm), and is altered depending on

its cell growth. The results show that neurons in the experimental set-up can live for at least 2 weeks, perhaps longer. Because the dry problem readily takes place when any microfluidic culture platforms are used, we invented the customized chamber with 3 types of water hole to keep neurons in the chamber. This chamber was designed based on the knowledge that the evaporation rate is dependent on its surface. The microfluidic chamber was downsized into the size of 19 mm inner ring on the MEAs, such that hole size of the small microfluidic culture platform is less than 3 mm diameter. Therefore the evaporation rate in the microfluidic outside is 6.5 times greater than in the microfluidic inside because the outside surface is about 183.385mm^2 and the exposed microfluidic surface is 28.26mm^2. And the customized cap was installed on the MEAs rings. It is known that convection of gas in the chamber from injected carbon dioxide and heat gives rise to the evaporation of media in microfluidic culture platform. The cap on the MEAs rings plays a role to minimize this convection. And the cap also has a small donut-shaped water hole to reduce the media's evaporation. Moreover, there is another main water hole on the preamplifier. It chiefly maintains the humidity in the chamber. Therefore the media in the microfluidic culture platform does not dried up at any more and the neurons in the system could be cultured for 2 weeks in the chamber. The neurons are vivid for 2 weeks as shown on Figure 2.3.

Moreover, the system is useful to observe axonal behavior exclusively and to monitor neural signals in developing neurons. The microfluidic device reported previously enables to separate soma parts in micro-channels and

axonal parts in micro-grooves. And it has advantages that make it the way a researcher wants. Therefore this system could be designed to measure only axonal behavior using this microfluidic device. Axons extended into the micro-grooves as early as 2 days after plating cells. They grew through all 800 μm microgrooves within 3 to 4 days. All axons in microgrooves were electrically active. Spontaneous spike rates between 2 and 10 Hz were recorded at all the electrodes in micro-grooves for 2 weeks while they were estimated at 10 of the 20 electrodes in micro-channels. And the background noise ranged from 10 to 50 μV peak-to-peak when 30um diameter electrodes are used. We used the system to discover that the neural signals had differences in time of first appearance and their amplitude when neurons developed and axons grew into microgrooves. The neural signal from neurons in the microfluidic microgrooves emerges approximately 2~3 days earlier. The neural signal at the electrodes in micro-grooves firstly appeared on 3 days *in vitro* while the neural signal at the electrode in micro-channels began to generate on 6 days *in vitro*. Moreover, the neural signal that was found in the micro-grooves was continuously increasing, on the other hand, while the signal that occurs from the micro-channels was saturated increasing slowly. In addition, the peak-to-peak in the microgrooves was 5~6 times grater than in the micro-channels. The peak-to-peak value in the micro-grooves was increasing continuously from 100 μV to 1600 μV as shown on Figure 2.3. However, the value in the micro-channel seemed the same tendency of spontaneous spike rate. It converged to constant value less than 200 μV.

Chapter 3. Optimum visible light parameters for focal photolysis of commercial caged glutamate to evoke neuronal action potentials

3.1. Introduction

The concept of caged compounds has set up the first specific practical technique of photo-stimulation. A molecule of interest is conveyed to a cell or tissue with an inactive state modified by chemical protection. It is defined as “caged”. These caging groups are covalently bound to the molecule, blocking its activity. The function is restored when the bond is cleaved by light irradiation. Some of these caging groups were applied in neurotransmitters, but very few of these caged neurotransmitters satisfied all the requirements of the neuroscientist for photolysis in complex biological tissue. The absorption of light by the caging groups led to the cleavage of the bond between the caging group and the neurotransmitter and the release of the neurotransmitter. These materials target ligand-gated receptors to open the channel and depolarize the membrane. Several protecting groups like nitrobenzyl, benzoin, (coumarin-4-yl)methyl, 7-nitroindoline, and p-hydroxyphenacyl derivatives have been coupled to neurotransmitters such as glutamate. These protecting groups are considered to be highly soluble and

stable in any aqueous solution. Poor stability can also lead to spontaneous release upon reaction with water. It is also important to consider the properties of the caging group, such as the molar extinction coefficient ε and the uncaging quantum yield ϕ. The quantum yield ϕ is a measurement of how many covalent bonds are cleaved per photon of incident light. The molar extinction coefficient ε relates the absorbance of the caging group to its path-length and concentration. If a cell has a 20 μm diameter, and the quantum yield and extinction coefficient of a caged compound are 0.09 and 5120, respectively, then the concentration of the caged compound should be more than 10 mM. In this way, the size of $\varepsilon \times \phi$ limits the application of the caged compound. The more important thing is that the value is dependent on the wavelength. The molar extinction coefficient is defined at a given wavelength. All caging groups have a wavelength range where cleavage will occur, and maximum cleavage can be achieved at a specific wavelength.

Some great scientific discoveries in neural circuit mapping have been accomplished with this photo-stimulation technique [68]. Optical stimulation with caged neurotransmitter can elicit action potentials on presynaptic neurons of interest, while intracellular recording is performed on postsynaptic neurons for the purpose of mapping their connectivity. This innovative technique was first applied to reveal synaptic connection in the visual cortex. A molecularly caged form of the neurotransmitter glutamate was bathed in brain slices [69]. A less than 1 ms pulse of ultraviolet light (UV) converted it into its activated form near presynaptic sites, and the neurotransmitter then stimulated single postsynaptic neurons. Higher

resolution stimulation on a functional microcircuit in living mammalian brain slices was achieved, changing the existing photo-stimulation paradigm. Another experiment also used photo-stimulation with caged compounds to study local circuits in the visual cortex. This technique revealed that 1) multiple types of visual information such as motion, shape, and color converged in layer 4B of the visual cortex [70], 2) the laminar sources of the excitatory cortical input correlated with particular cell types [71], 3) input sources to the individual cells in layer 3B of monkey primary visual cortex were highly diverse [72], and 4) the two functional channels from the visual cortex to the visual cortical area consisted of different cell types [73, 74]. Optical stimulation with caged glutamate allowed the study of receptive field plasticity and its dependence on experience to rapidly map 1) the development of intracortical circuits onto layer 2/3 neurons in the rat's barrel cortex [75-77] and 2) the spatial distribution of functional excitatory synaptic input to individual L2/3 pyramidal neurons in the rat's barrel cortex for the specific location dependence of the functional organization of projections to L2/3 neurons [78-80]. This technique has been used most widely to study neural connectivity in not only the cerebral cortex, but also in the superior colliculus, the suprachiasmatic nucleus, and the hippocampus [71, 81-85].

Several scientific studies combined uncaging photo-stimulation and whole cell recording to mimic synaptic input in part or to map receptors [85]. One representative experiment in its early stage is the accumulation of knowledge about long-term depression (LTD) based on the glutamate

response [86]. Caged glutamate was able to produce new knowledge about 1) the localization of LTD on apical dendrites of layer 5 pyramidal neurons [87], 2) the distribution of NMDA and AMPA receptors on dendrites [88], and 3) the response to glutamate being non-uniformly distributed along the apical dendrite [89]; it was also determined that glutamate receptors have at most four hot spots responsive to glutamate.

Most notably, caged compounds are conventionally positioned in the middle of thick specimens, resulting in photolysis of caged compounds in untargeted specimens, i.e., too much neurotransmitter is released along the laser path above and below the focus. The light going to and from the focal point passes through a double cone of illumination parallel to the focal plane. The axial resolution is on the order of tens of micrometers, and even a focused UV light beam is guided to a diffraction-limited spot. Therefore, photo-stimulation with caged neurotransmitters has evolved for highly spatial or temporal resolution ever since it was successfully established. For example, flash photolysis was exploited to study living cells in real time. When caged glutamate was loaded and released into the cell, the reaction in response to light can be observed at any moment during the experiment in locally defined regions. A fiber optic guide to deliver light to the caged neurotransmitter *ex vitro*, *in vitro*, and *in vivo* was developed. Evoking action potentials in cat brain and rat brain slices was accomplished with caged glutamate and a tapered fiber light guide in a glass capillary. This flexible and feasible technique enables the recording of a physiological response to light exposure. A UV light-emitting diode was suggested as an alternative to

UV lasers. However, the light-induced stimulation with caged compounds was restricted by the diffraction-limited illumination system in making large cylindrical excitation volumes. However, two-photon excitation can be localized with a volume much smaller than one femto-liter. Two-photon photolysis of caged neurotransmitters releases the neurotransmitter at a single synapse; the activation of multiple synapses could be used to study information processing in neural networks [90]. For example, rapid multisite two-photon uncaging of glutamate enabled us to answer such questions as how the spatiotemporal pattern of synaptic input determines which properties of integration are to be engaged. Radial oblique dendrites in the hippocampus were artificially stimulated using two-photon glutamate uncaging technology; the signals were simultaneously recorded through two-photon calcium imaging and somatic whole-cell voltage measurements. The patterns of synaptic input were defined on a sub-millisecond and micron scale to investigate the rules for summation of synaptic inputs in the fine oblique dendrites of pyramidal neurons. This study argued that at least 20–25 synaptic inputs activated within 6 ms or less could evoke a dendritic spike [91]. The authors showed that a synchronous input pattern produced Ca^{2+} signals to mirror the voltage response. Moreover, the results revealed that the rapid initial phase of the dendritic spike was primarily delivered through a sodium channel, and that the slow phase was mediated by NMDA receptors.

A major objective of two-photon uncaging stimulation is to stimulate many spines of a neuron simultaneously in order to study synaptic function

and plasticity. For the photolysis of spot sizes over various ranges in a single, uniform, and circular area, a holographic illumination was applied to caged glutamate for AMPA receptor activation in brain slices and for multi-cell stimulation using a liquid crystal spatial light modulator. A three-dimensional stimulation system was also proposed for a multi-foci photo-stimulation pattern. Kasai H and his coworkers presented a new technology to map the synaptic connectivity and strength using two-photon photolysis of caged glutamate. Their technique could evoke an action potential in only a small number of neurons. They used a decreased numerical aperture of the objectives, resulting in an increase in the volume of two-photon excitation, allowing the stimulation of a large three-dimensional area on the single-cell level. A holographic projection of multiple focal spots was used, which allowed full control over the 3D positions of uncaging sites with a high degree of localized excitation. The system incorporates a two-photon imaging setup to visualize the 3D morphology of the neurons in order to accurately determine the photo-stimulation sites. The system was applied to studies of synaptic integration by performing simultaneous and controlled glutamate delivery at multiple locations on dendritic trees.

Despite the numerous studies using photolysis of caged glutamate, remarkably few systematic investigations and quantitative analyses have probed the efficacy of caged glutamate over various combinations of pulsing parameters. In addition, the light source for almost all of the studies using photolysis of caged glutamate was UV, far removed from the visible source that is usually installed for fluorescent imaging in microscopic systems.

Moreover, the response of a single neuron to the photolyzed glutamate is still unknown in high-density cultures.

Here, we studied photolysis of common commercially caged glutamate intended to elicit action potentials of cultured neurons on MEAs coupled with microfluidics. The results in this paper were obtained from stimulating and monitoring neural activity at the same time, and then analyzing the neural response using a spike-sorting technique. The results showed that the neural response to the glutamate released by irradiation of visible light was dependent on wavelength. In addition, we suggested the effective optical parameters of the common commercially caged glutamate as a function of exposure time and intensity. Furthermore, the latency analysis indicated that the response was classified into late post-synaptic spikes that relied on glutamergic synapse, and occurrences exceeding 100 ms after stimulation.

3.2. Methods and materials

MNI-caged glutamate was bathed in the warmed neurobasal media for neurons in the microfluidic channels. The dissociated neurons were cultured in a microfluidic device combined with planar MEAs for 2 weeks. When a single pulse of continuous visible light was applied into them, it decomposed the caged glutamate, such that released glutamate to bind with downstream effectors and evoke action potentials.

The intensity and the exposure time of light were regulated by the controller of continuous visible light ranging from 300–600 nm LED (SOLA

light engine, Lumencor). We drew up a control program based on the software of LabView in a PC. It is connected to the controller using RS-232 protocol. Additionally, it used internal counter and loop commander to control the exposure time. The graphic-based user interface provides us the regulation of periodic time, exposure duration, and light intensity as well as wavelength.

3.3. Results

Photolysis of caged glutamate, as one type of optical stimulation, changed the neural activity of the stimulated neurons. For the analysis of single neuron's response, we selected one kind of spike among the entirety of spikes that emerged from the irradiation, using the spike sorting technique as previously explained, and then calculated the variation of the number of spikes between pre-stimulus and post-stimulus. The analysis showed regularly evoked action potentials when it was irradiated into electrodes in the micro-channel in which the soma was located in the microfluidic device. Figure 3.1(a) and 3.1(b) showed that the evoked action potential was less than a second long, and the spontaneous activity recovered in time. Moreover, the evoked spikes were recorded in both the soma and axons periodically, such that the time interval between the stimulation and its first response was regular, at approximately 100 ms, shown in raster plots (Figure 3.1(e), 3.1(f)) and peri-stimulus time histograms (Figure 3.1(g), 3.1(h)).

To explore how the optical stimulation affected neural activity, we

analyzed the spike waveform, which contained information on the biophysical mechanisms of action potentials near extracellular recording electrodes, and the membrane properties of the recorded neurons. Figure 3.1(c) and 3.1(d) show that the waveform of the aligned and overlapping spikes in response to the optical stimulation are commonly biphasic. The response of one-photon exogenous stimulation is composed of an initial dominant positive peak followed by a negative peak. The first positive peak is larger and narrower than the negative. The spike thereafter slopes from side to side.

Figure 3.2(a) shows the UV-Vis spectrum of the commercial caged glutamates recorded in the neurobasal media supplemented with B27 and GlutaMax. The experimental data indicate that MNI-caged glutamate is not only sensitive to the UV light, as is already known, but also to visible light, the same as RuBi-caged glutamate. The calculated absorption spectrum for MNI-caged glutamate has a weak peak at the centered wavelength, which means that the yield of photoreleased glutamate can stimulate excitatory neurons in the hippocampal culture using visible light with MNI-caged glutamate. To determine the relationship between photolysis of caged glutamate and wavelength, we observed the neural response elicited by photolysis of MNI-caged glutamate using 4 different wavelengths – 405 nm, 445 nm, 480 nm, and 520 nm at a fixed light intensity of 90.5 mW for a 500 ms duration, as shown in Figure 3.2(b). When the light differed in wavelength, the spikes were analyzed a second after exposure. The 405 nm wavelengths evoked about 3-spikes per second, while the 445nm, 480 nm

and 520 nm wavelengths did not change the number of spikes. The results were well matched with the tendency of UV-Vis measurement. Based on these wavelength results, we selected only the 405nm wavelength light for photolysis of caged glutamate.

To investigate whether there is a threshold level of pulse duration and power intensity for the photolysis of caged glutamate, we conducted a sequential set of experiments with more acute parameters in which light at a wavelength of 405 nm was irradiated into neurons. Figure 3.3(a) suggests that a critical factor of optical parameters is light dose multiplied by pulse duration and light intensity. The threshold level is constant over radiant exposure. The spikes evoked by photo-released glutamate began to emerge at 1 mJ at 4 mM MNI-caged glutamate. Moreover, the threshold level was dependent on the concentration of MNI-caged glutamate bathed in neural basal media. 1.5 mJ exposure dose at 2 mM MNI-caged glutamate was enough to evoke spiking, while 3 mJ at 1 mM caged glutamate was required.

The average spike counts per second were also increased, depending on optical parameters. To further characterize the performance of caged glutamate for neuronal excitation, two parameters, power intensity and duration time, were applied into cultured hippocampal neurons with a single pulse. To compare the responses from the same neuron, we used the spike sorting technique to extract the spike waveforms and analyzed them with MATLAB software (Mathworks, USA). To study the effect of light intensity on spike rate, we performed light exposure using an available range of intensity, shown in Figure 3.3(b). More than 10 exposures per condition

were performed on the same individual neuron while the intensities and the duration time were varied. Less than 6.2 mW of light with a 400 nm wavelength could not depolarize the membrane potentials of the single neuron. Light providing more than 30.5 mW of intensity and with exposure durations of at least 50 ms began to increase the spike rate per second. The variation in spike number increased linearly when more intense light was applied, and ranged from 1 to 3. To assess the impact of light intensity, we determined the effect of exposure durations ranging from 10 to 500 ms. More than 50 ms of exposure time was necessary to activate a single neuron at a fixed light intensity of 30.5 mW. The variation in the number of spikes in the stimulated neuron is also proportional to exposure time.

Another approach that neurons use to communicate information is believed to be the use of spike timing – considering exactly when spikes occur within the time window. The first-latency information in a single neuron is one of the representative tools to uncover the role of spike timing in the spike trains. To acquire exact latency information, we calculated the time of the first spike after stimulus. The dataset previously recorded of all neurons responding to photolysis of caged glutamate was used to investigate the role of spike latency occurrences. The majority of neurons showed that the mean value of the first spike latency was 198.7 ± 2.43 ms. The exposure time required to elicit action potentials at a fixed intensity 174.9 mW was a minimum of at least 20 ms. The delivery time of action potentials to the axon was less than 1 ms in about a 500 μm microgroove in the microfluidic device, because the velocity of axonal propagation in the microgrooves is known to

be 0.5 ± 0.1 m/s. Considering these factors, the response latency of glutamate released by photo-stimulation is approximately 100 ms. Since the delay from the breakdown of caged glutamate using visible light is less than the exposure time, the post-synaptic process likely contributes to the delayed response of caged-glutamate. Previous studies revealed that the NMDA receptor was more affected by later onset spikes than the AMPA receptor was, while both the AMPA receptor and NMDA receptor were effective in short latency (<12 ms). These data suggest that the delayed latency excitatory response to photolysis of caged glutamate using visible light may be mediated primarily by NMDA receptors.

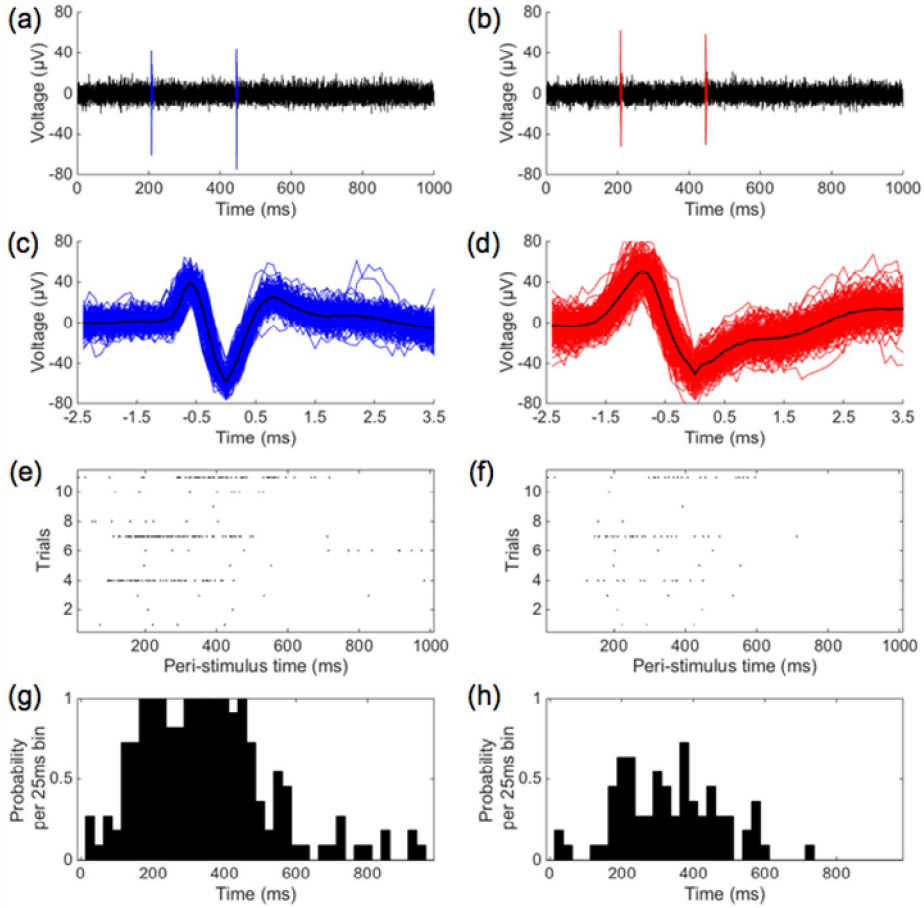

Figure 3.1. Raw data, aligned spike waveform, PSTH, and raster plot in response to photolysis of MNI-caged glutamate. The response to photolysis of caged glutamate emerges from soma in a microchannel (a) and axons in a microgroove (b). The spike waveform recorded from the electrode in a microgroove (d) was primarily composed of one positive peak and one negative peak, while the response of the electrode around soma (c) has the first small positive peak, the second big negative peak, and the last small positive peak. These spikes were measured from the same animals.

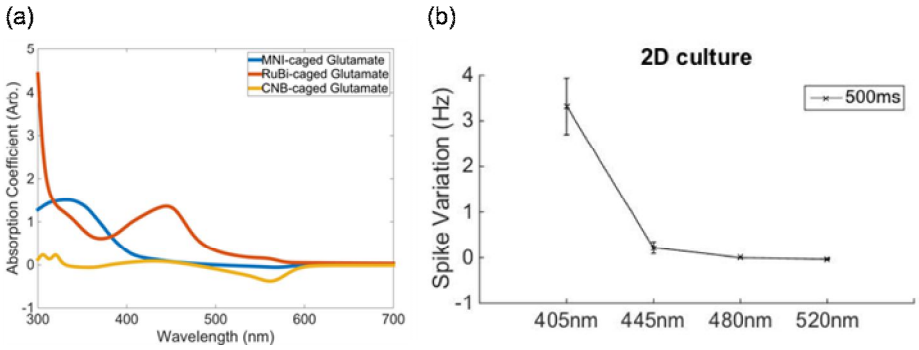

Figure 3.2. Wavelength variability of neural response evoked by photolysis of MNI-caged glutamate. (a) Absorption coefficient measured with UV-Vis spectroscopy (b) Spike variation decrease at longer wavelength. Wavelength between 405 – 520 nm were examined. The average data with standard error bars are shown in black squares. Each type of data marker represents average value on a different neuron. ($n \geq 10$)

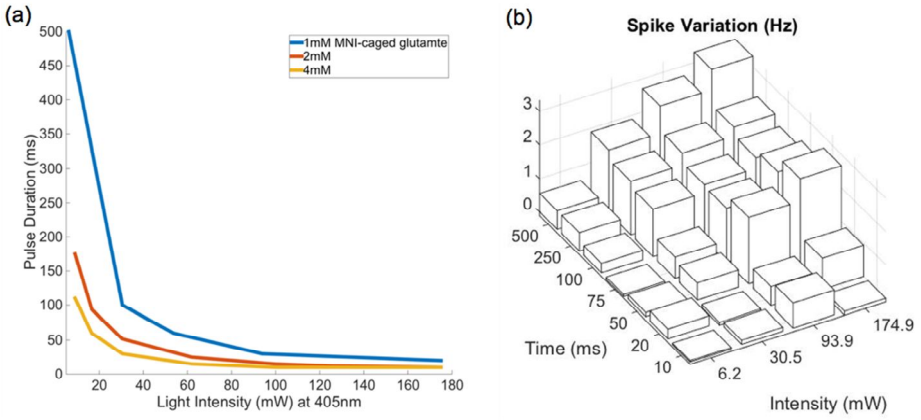

Figure 3.3. Stimulation threshold for various intensities and pulse durations and 3D graph of spike variation with intensity and exposure duration. (a) The stimulation threshold is constant over radiant exposure. However, it is dependent on MNI-caged glutamate's concentration. (b) The spike variation increases with increasing intensity and pulse duration. The individual data sets, each measured from the same neuron, are shown by the 3D bars.

3.4. Discussion

In conclusion, we used visible light to produce action potentials in cultured neurons. We set up a customized system to combine a microfluidic culture device with microelectrode arrays, which optically measure neural signals of cultured neurons. We utilized the commonly used caged glutamate to stimulate down-effectors of neurons and to evoke action potentials. We found that, these methods of stimulation increased the count of spikes per second when the soma of neurons were exposed to the focused light in the microfluidic device. Their detected spike waveforms, classified by the polarity of their largest peak, showed mainly positive first biphasic spikes. The results imply that optical stimulation and microelectrode measurements in microfluidic culture systems may be a useful tool for the application of a driving stimulus that can depolarize single neurons, facilitating the investigation of their response in neural networks where other methods cannot be used or are unable to achieve the same level of subcellular localization. Using this differential spiking pattern, our system could prove very useful for the analysis of neural network connectivity. In addition, the spike timing analysis revealed that it took more than 100 ms for the neurons to respond to photolysis of caged glutamate through post-synaptic glutamate receptors. It was supposed that its process might pass predominantly through NMDA receptors.

Chapter 4: Endogenous neural stimulation using the focused femtosecond laser

4.1. Introduction

Direct optical stimulation of unmodified neurons without any exterior materials was first described in 1994 [92]. Several studies at that time had already reported the neural response to a continuous laser and the influence of visible light on the spiking rate of a single cell. It was reported that the crayfish stretch receptor neurons were stimulated using a pulsed periodic visible light laser [93]. The authors observed that the spiking rate first increased and then decreased under irradiation. It was also found that the firing rate quadratically depended on the peak beam intensity during the firing acceleration phase. The authors suggested that this finding indicated the participation of a two-photon process. The first direct proof was presented in 2002 [94]; light irradiated with a pulsed femtosecond laser was able to generate a series of action potentials in a single neuron. Pyramidal neurons from the visual and somatosensory sections of a mouse brain slice were used. The laser source was a titanium (Ti):sapphire laser providing 130-fs pulses at a 76 MHz repetition rate. In their experiments, low-intensity light pulsed from a mode-locked infrared laser was introduced for imaging, and a high-intensity laser was used for stimulation. They demonstrated that the laser-induced depolarization depended on its location, average power,

and wavelength. The irradiation of the proximal apical dendrites did not evoke depolarization, unlike those of the soma. The irradiated position was constrained to the region of the somatic membrane. A higher power could produce more action potentials, whereas a laser of less than 250 mW led to a negligible depolarization of the neuron. Moreover, this two-photon stimulation without any exterior materials occurred only if the pulsed laser emerged from the mode locking..

Recently, two teams applied a two-photon intrinsic stimulation to single-cultured neurons. One team set up a mode-locked laser with a pulse width less than 100 fs at 82 MHz and 800 nm center-wavelength [95]. The laser was set to 5 mW for imaging and 40 mW for stimulation. The stimulation period ranged from 50 to 200 ms. When the beam was introduced to the hippocampal neurons in the culture, the authors observed an increase in the calcium level in a single neuron for 1–2 seconds. Another team improved the experimental setup by combination with a confocal microscope and a commercialized multi-electrode array recording system [96]. The laser was set to 5 mW for imaging and 40 mW for stimulation. The stimulation period ranged from 50 to 200 ms. When the beam was projected on the hippocampal neurons in the culture, the authors observed an increase in the calcium level in a single neuron for 1–2 seconds. Another team improved the experimental setup by a combination of a confocal microscope and a commercialized multi-electrode array recording system. They also used a mode-locked Ti:sapphire laser beam with a 100-fs pulse duration, 82-MHz repetition rate, and 800-nm center wavelength. The

beam size was expected to be 0.98 μm2 at an average power of 30 mW. The researchers observed that the calcium level in the neurons increased upon irradiation with the femtosecond laser with an average power of 20 mW. They showed that the two-photon stimulation had threshold values of average laser power and irradiation time using the Ca^{2+} imaging technique. It was also observed that the two-photon stimulation depended on the position of the focal point. In addition, they confirmed the evoked action potentials induced by the two-photon stimulation using a multi-electrode array recording system.

Direct optical stimulation is currently effective. However, it is still an imprecise way to stimulate neurons and may cause off-target effects or cellular damage. Moreover, there is no report describing stimulation of neurons in 3D environments. The mechanism underlying the neural response evoked by the femtosecond light is still unclear. Therefore, further experiments demonstrating that the light depolarizes action potentials under normal physiological condition, and investigating the properties of neural response are required.

4.2. Methods and materials

The laser source was a Ti:Sapphire laser (Cameleon Ultra, Coherent, USA) of 700 nm radiation, mode-locked to generate 140 fs pulses fixed at an 80 MHz repetition rate. The laser beam delivered into the back port of an inverted microscope (IX70, Olympus) to allow laser irradiation. A beam

expander was used to fill the aperture of a 60x/0.7 NA objective lens. The laser power was measured at the focus passed through the objective lens by a power meter. The laser irradiation timing was controlled by a mechanical shutter (SH05, Thorlabs, USA).

4.3. Results

4.3.1. Identification of the neural response to ultra-short pulse light

The activation of a single neuron by irradiation with femtosecond light was monitored in a microfluidic device combined with planar microelectrode arrays on an inverted microscope. The cultured hippocampal neuron was visually identified through a microscope imaging system and exposed to the femtosecond light. When we exposed a single neuron to the light for less than 10 ms (<70 mW at 700 nm, Figure 4.1(a)), we found that the evoked spikes also occurred constantly for a second, and then rapidly at a regular rate (Figure 4.1(b)). The neuron's firing by the femtosecond light reaches the critical level to initiate membrane depolarization. There are three controllable factors for the light: wavelength, power intensity, and exposure duration. To investigate how long or how strong the femtosecond light depolarizes the neuron's membrane potentials, optimization of the laser parameters was undertaken by varying the laser power and exposure time, while keeping the wavelength constant (700 nm). The probability of the

generation of response to the femtosecond light in a neuron has already been reported in previous studies. It was a function of the average laser power and laser irradiation time. However, we excluded the probability and calculated the number of spikes per second after stimulation when the neuron was only activated. We plotted the number of spikes evoked by the femtosecond light with different laser exposure durations and power intensities by an individual neuron in the same sessions (Figure 4.4.). We found that the light irradiation drew a threshold curve, yielding a steep curve at the point of initiation of an effect. The 20 mW and 46 mW femtosecond light could activate a neuron at durations of more than 100 ms and 50 ms, respectively. In contrast, light with 86 mW and 110 mW power began activating a neuron over a duration of 10 ms. Both 156 mW and 180 mW induced a response from durations of 5 to 20 ms. At higher average laser powers (above 156 mW) and longer duration (above 20 ms), cell death was observed, showing significant morphological changes like membrane explosion. Notably, once the neuron was activated by the femtosecond light, almost 20–30 spikes per second were generated regardless of the variables. The polydimethylsiloxane (PDMS) microfluidic device is a tool with physical barriers that confines somas to compartments and isolates axons *in vitro*. Combined with the planar microelectrode-arrays, it can record neural signals from axons in microgrooves. We used this PDMS technique to demonstrate that the neural response to the femtosecond light emerged only from irradiating the soma in the neuron (Figure 4.3.). When the soma in the micro-channel was exposed to the femtosecond light, the repetitive spikes occurred as representative

responses. In contrast, when we irradiated the axon in the microgrooves with the femtosecond light, we did not measure any response including repetitive spikes.

The neural signals recorded from the soma show the characteristics of having an almost mono-phasic, negative-first spike points at the origin of the neural response to the laser irradiation (Figure 4.2). To examine whether the response comes from the soma, we recorded the spike activity in 64 channels on a planar microelectrode-array (MEA) while irradiating with the femtosecond light and sorted all the evoked spikes in the electrode near the stimulated neuron. The evoked activity of a single neuron exhibited repeated waveforms in response to the laser irradiation. The average was obtained by overlaying all the spikes and by aligning them to the negative peak and plotting a median trace. The shape of the laser-induced current response was seen as the negative-first spike. It was different from the spike characteristics observed at the axons in the microgrooves, consisting of a large positive peak followed by a large negative peak, and then a third small positive peak. The spike amplitudes were as indicated by the scale bars. The recordings thus support the idea that only the soma of the neuron responds to the femtosecond light.

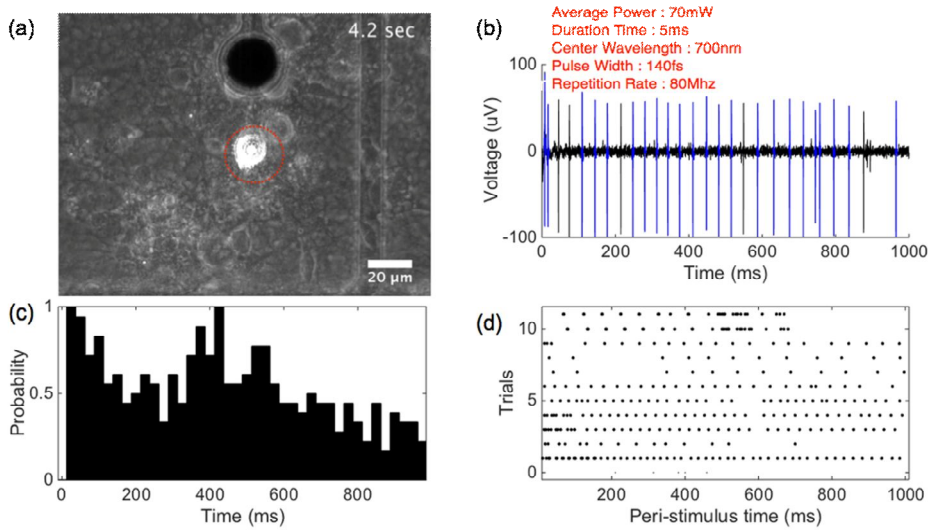

Figure 4.1. Neural response to irradiation by the femtosecond light. (a) Photo image of a single cell stimulation using the focused femtosecond light (b) Raw signals of the responses evoked by a brief 5-ms light pulse shows repetitive spikes. The blue color represents spikes having the same waveform (c) Raster plot, (d) Peri-stimulus time histograms of a neuron optically activated with a 5-ms light pulse without the addition of any exterior materials. This experiment was performed in the new microfluidic system, as previously explained in the Methods.

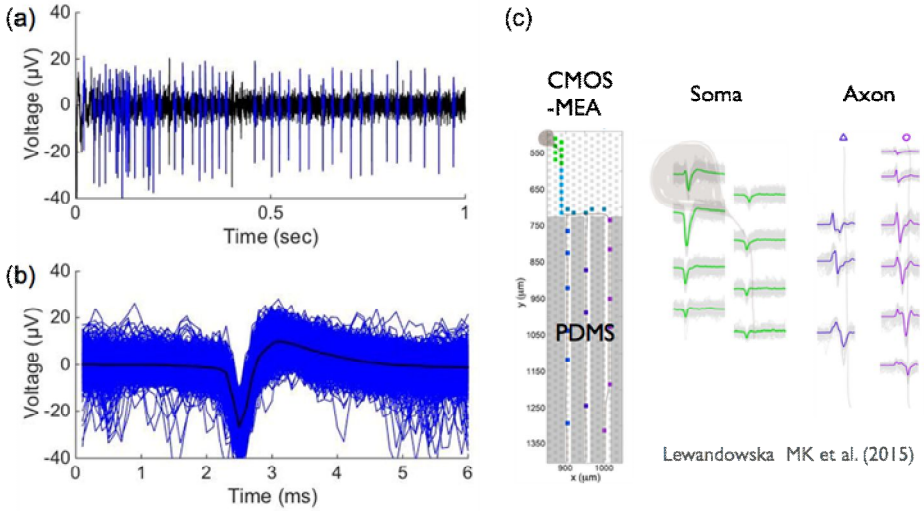

Figure 4.2. Example of voltage traces and their waveforms of action potentials induced by the focused femtosecond light. (a) The spike trains of neural responses evoked by a 5-ms and 70-mW light pulse show repetitive spikes. (b) The extracted spikes (blue) show a common waveform of a negative and then, a positive shape.

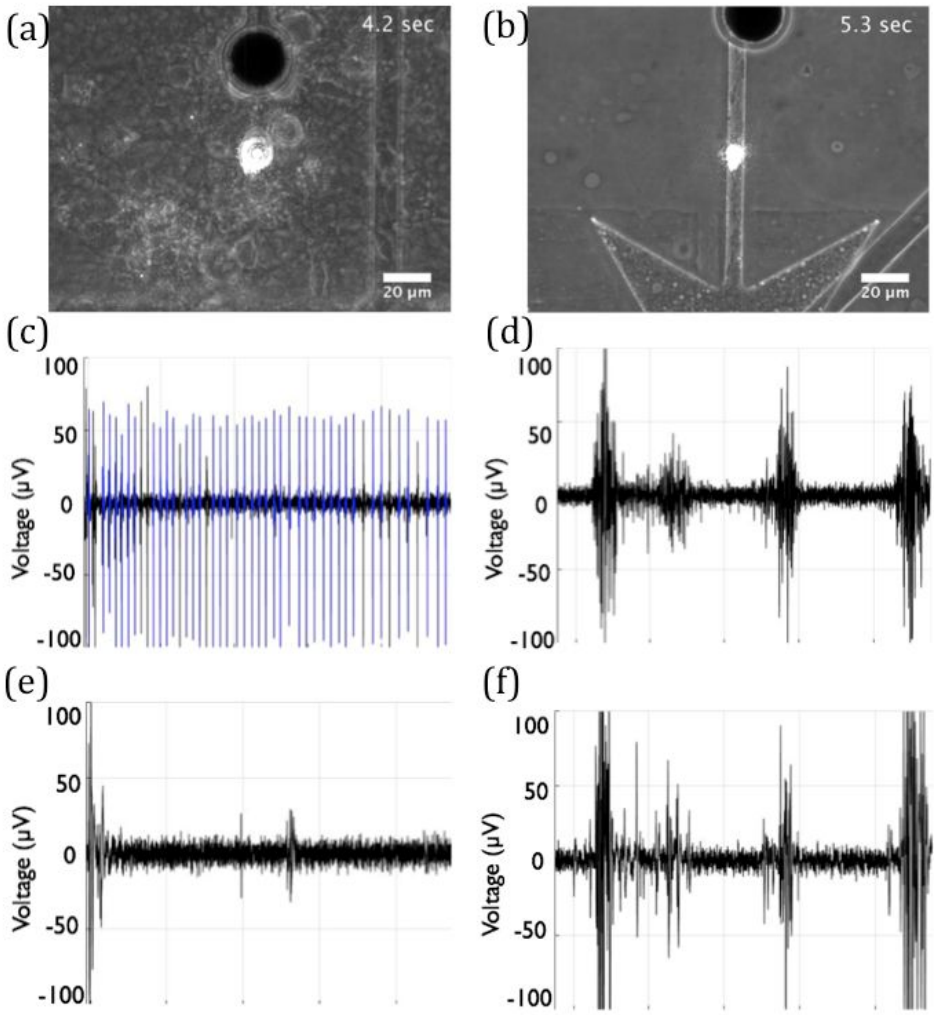

Figure 4.3. Position dependency of photo stimulation. A neuron responds to ultra short pulse light when only the soma is irradiated. (a) Figure of light exposure at the soma in a micro-channel (b) Figure of light exposure at the axons in a microgroove (c, e) Neural response of soma (c) and axon (e) and when the soma was exposed to ultra short pulse light (d, f) Neural response of soma (d) and axon (f) and when the axon was exposed to ultra short pulse light

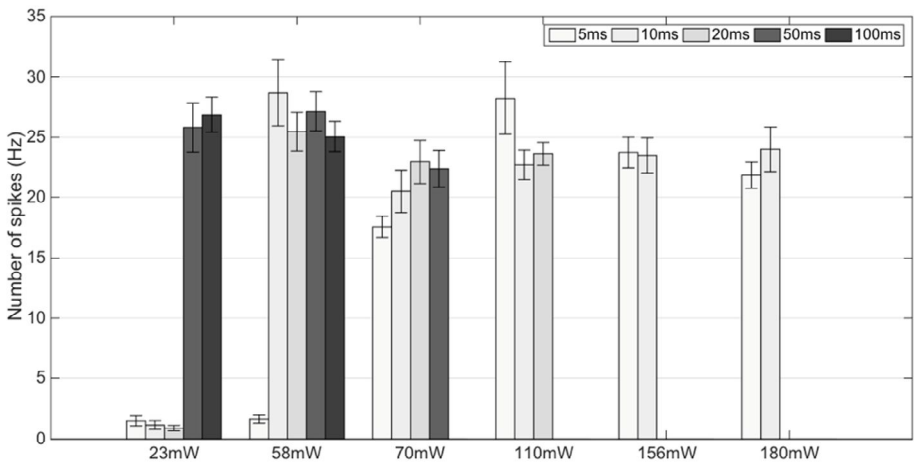

Figure 4.4. Spike rate in response to the femtosecond light. Once activated, neurons generate repetitive spikes of 20–30 Hz, irrespective of the pulse duration and power intensity.

4.3.2. Endogenous neural stimulation for 3D neurons

To determine if the femtosecond light can be biologically applicable, we investigated the spatiotemporal resolution of the femtosecond light as an alternative to neural stimulation. To achieve a high resolution, we utilized a high power objective lens, which allowed for precise and localized photo-activation of a neuron. Because our microscope apparatus used a 60X 0.7 N.A. objective, the Gaussian waist size was calculated as approximately 0.909 μm at 700 nm-centered wavelength (Gaussian full width at half maximum [FWHM], 0.773 μm) and the Rayleigh length was 3.710 μm, resulting in a cylindrical volume of 1.534 μm3 (± 10%). The spot size of the focused beam was enough to irradiate the soma of a single neuron with a diameter of 5–10 μm in the 2D culture. Therefore, the effect of the two-photon irradiation theoretically ranged over a subcellular area.

For temporal control of firing in the individual neuron, the mechanical shutter was used to control the irradiation time. It supported an exposure time of more than 5 ms with less than 100 Hz repetitions. A single pulse of focused femtosecond light was used for more than 5 ms to stimulate neurons with 1 ms as a unit.

Multi-site stimulation abilities based on the microscope system allow the possibility of manipulating the activity of multiple neurons for a short time. For sequential activation of more than two neurons with intervals of >1 sec, we steered the microscope stage and moved the laser spot to the next neuron after triggering the spikes in the first neuron. In this case, the evoked

spikes in the two electrodes closely followed those observed for the sequential femtosecond light irradiation.

One concern with light manipulation of neuronal activity is the potential photo-damage mediated by the femtosecond light. During this study of repetitive stimulation, neurons were optically stimulated to produce spikes with no evidence of toxicity or cellular damage induced by the optical stimulation. In our system, the femtosecond laser was focused on a spot (~ 1 μm) in the focal plane. The individual neurons were reliably excited with a laser pulse with a power of <70 mW and an irradiation time of <10 ms, for a total energy load of <7.84 nJ, which was much lower than those associated with the previously reported two-photon excitation experiments. The responses to the femtosecond light were strong and reproducible as shown in Figure 4.1(c) and (d).

When femtosecond light with more than 5 ms duration at 170 mW was focused onto a neuron, we observed that something appeared and disappeared. Because the spatial resolution $R = 1.22\lambda$ / (N.A. [objectives] + N.A. [condenser]) is less than 0.5 μm, only a change in the cellular morphology of more than 0.5 μm can be detected in the system, seen as a micro-hole or a bleb. The micro-hole is defined as a single transient hole in the neural membrane or cellular organelle that lasts for a few milliseconds. Several hypotheses on how the femtosecond light forms the micro-hole has been proposed, but the mechanism remains unclear. The femtosecond light has been previously reported to make a micro-hole in the cellular membrane, which has been applied in drug-delivery systems for optoporation in

relatively high-throughput studies. However, we do not have any obvious evidence that the femtosecond light created a micro-hole in our experiments. It may be a bleb. A bleb is a protrusion of the cell membrane where the membrane is transiently decoupled from the actin cortex. It also transiently appears, similar to a transient hole. Taking into account the cylindrical volume of the focused femtosecond light with a diameter of 0.909 μm and length of 3.710 μm, the light could detach the membrane. A recent study also reported that the focused femtosecond laser formed a bleb on the plasma membrane. The bleb formation was acknowledged as one of the typical cellular symptoms of the execution phase in apoptosis. However, the specific role of blebs is still debated. Blebs are often observed in healthy cells. Several types of cells without lamellipodia apply blebs for their migration; this is called "blebbing motility." Therefore, it cannot be concluded that the membrane bleb formed by the femtosecond light damages the neurons without clear evidence.

The irradiation by the femtosecond light at 70 mW for less than 10 ms did not cause any changes in the cellular membrane, while activating the cultured hippocampal neurons. Despite the micro-hole (or bleb), the morphology or neural activity of the stimulated neuron was not changed. Indeed, for 24 hours after the laser irradiation of the single neuron, no obvious change was found in the morphology or the cellular membrane of the stimulated neurons (Figure 4.6.). The laser stimulation of the same neuron after 24 hours repeatedly generated a similar response to that before 24 hours. On the contrary, a single stimulus with a laser pulse of >170 mW

power and a duration > 20 ms instantly killed the neuron (likely due to overheating). In conclusion, the femtosecond laser irradiation of a low power and short duration is an efficient and safe method for activating a single neuron (Figure 4.5).

We also examined the method for controlling the spiking activity in a 3D culture. The 3D neuron culture was established by injecting hydrogels mixed with cells into the microfluidic device (see Methods). The activity of the 3D hippocampal neurons was successfully recorded by a planar 60-channel MEA combined with the microfluidic device. Their spontaneous signals were recorded in the mature phase of their development (i.e., after 3 weeks *in-vitro*). The electrophysiological activity of the neurons in the 3D culture was then analyzed with the same spike sorting and compared with that of the 2D hippocampal culture. Further analyzing the raw data of a single channel, we found that most of the burst spiking in the 3D culture was longer than that in the 2D culture neurons (Figure 4.7.). As reported in the literature, the 3D hippocampal neurons in the microfluidic device showed similar activity characterized by longer duration bursts as well as significant random spiking, non-synchronous bursts. To demonstrate whether the femtosecond light stimulated a neuron in the 3D culture, we performed experiments by delivering the femtosecond light.

Because we were not able to directly see the individual neuron in the 50 μm thick gel, we stimulated from the bottom layer and found the position that had a regular reaction of neurons to the femtosecond laser. When the femtosecond light irradiated the 3D neuron, the rapid spike trains occurred at

a regular rate for a second similar to the stimulation of 2D neuron (Figure 4.7(a)). Interestingly, the applied stimulation on the 3D neuron evoked neural activity with a longer burst of spikes (Figure 4.7(b)). Figure 4.7(c) and 4.7(d) show the peri-stimulus time histograms (PSTHs) and the raster plot of the neural responses to the femtosecond light, repectively. The PSTH profile demonstrated the reproducibility of the optical stimulation using the focused femtosecond light. The response with the laser exposure occurred in approximately 60% of all trials for an average power of 70 mW and 10 ms duration without cellular damage. The highest response peak (i.e., the maximum of the evoked response) was detected around 250 ms after the stimulation. These results indicated that 60% of the response was within the first 300 ms after stimulation. Considering the average time of the first response was about 50 ms in the 2D neurons, the response in the 3D neurons may have additional signal pathways within the cellular organelles.

Irradiation by the femtosecond light induced neural activation similar to other neural stimulation methods such as electrical stimulation and photolysis of caged glutamate. However, the neural response to the femtosecond light showed different features (Figure 4.8.). We used the electrical stimulation (Figure 4.8(a), 4.8(d)), photolysis of caged glutamate (Figure 4.8(b), 4.8(e)),, and femtosecond light (Figure 4.8(c), 4.8(f)), to activate neurons in the same sample. For detecting the response of the same single neuron, all neural signals recorded with the planar microelectrode-arrays were analyzed using the spike sorting technique as described previously. Photolysis of MNI-caged glutamate caused a glutamate-mediated

elevation of neuronal spikes in the cultured neurons. To see whether glutamate released by visible light alters their activity, we used a 400 nm LED violet light to irradiate the cultured neurons for 100 ms. The time course of axonal response after the visible light exposure showed a significant increase in the spike number to 0–10 spikes per second. The soma and axon's response to photolysis of caged glutamate was regular. Similarily, electrical stimulation activated both the soma and the axon. Their response times were regular for the stimulated time, similar to the photolysis of caged glutamate. The number of evoked spikes ranged from 0 to 60 per second, depending on the current intensity and duration. In the case of the femtosecond light, only the soma responded with spikes increased to 20–30 per second. The response was irregular and the spikes were generated at a rapid rate. Importantly, the latency of the spike response was different from each method. We found that the electrical stimulation or photolysis of caged glutamate produced precisely timed spikes across multiple repetitions. The latency value of the photolysis of caged glutamate was 198.7 ± 2.43 ms, and that of the electrical stimulation was 13.6 ± 3.43 ms. The latency of the electrical stimulation was well matched with the latency of the direct response that does not depend on glutamatergic synapses. The latency of glutamate that binds in post- synapse, released by photolysis with visible light was slower than that of early onset post-synaptic spikes. It is assumed to be associated with the NMDA receptor. Contrary to these, a series of spike trains irregularly occurred at the onset of the femtosecond light. The latency of the femtosecond response was on average considerably shorter than that

of the photolysis of caged glutamate, and longer than that of the electrical stimulation. It is likely that this latency difference arises because the neural response to stimulation passed through different organelles.

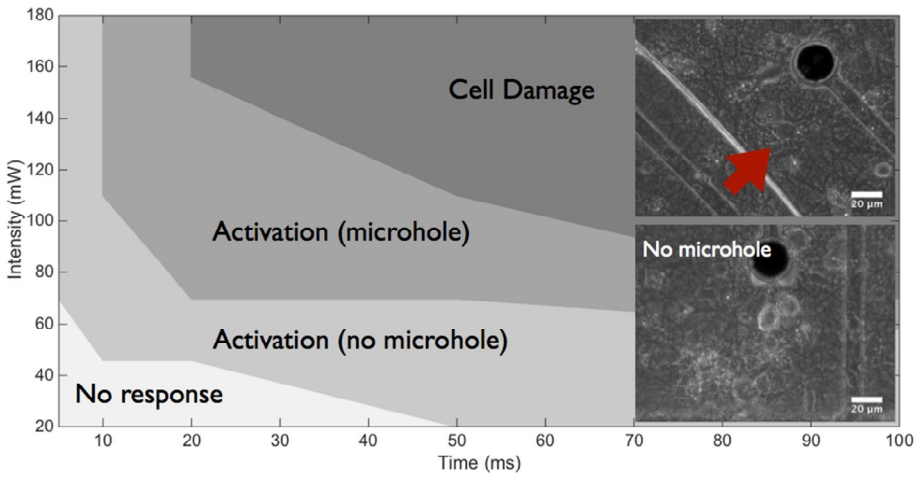

Figure 4.5. Phase diagram of power intensity and pulse duration. There is a safe range of stimulation parameters that generate the repetitive spikes in response to irradiation of focused femtosecond light without cell damage.

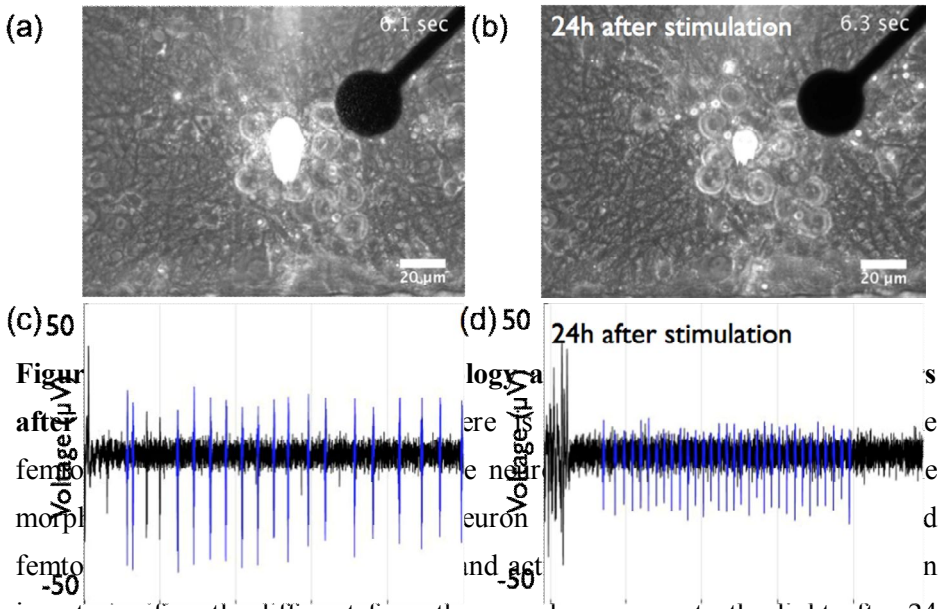

Figur **logy a** **s**
after ere e
femto e neur e
morpl euron d
femto nd act n

is not significantly different from the neural responses to the light after 24 hours. Only the interval between spikes after 24 hours is much smaller.

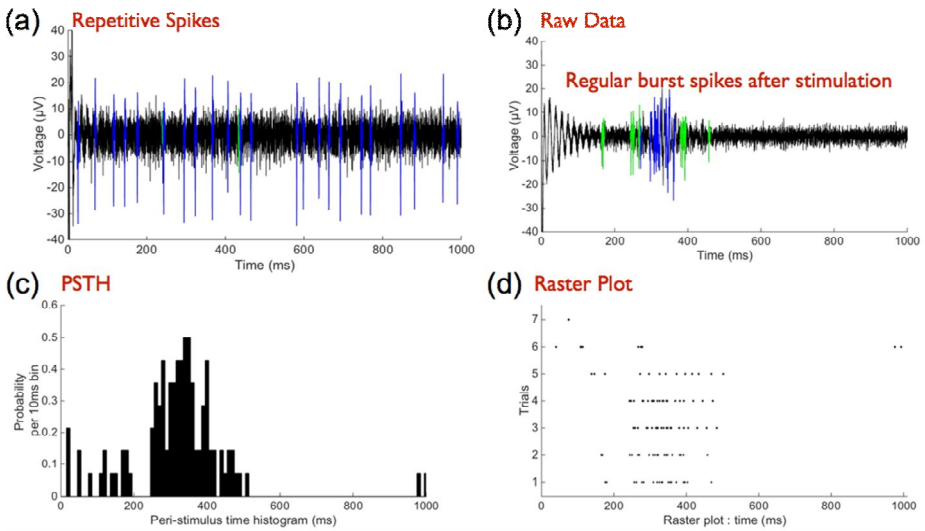

Figure 4.7. Results of a femtosecond stimulation in a 3D culture. When we stimulate a neuron in a 3D microfluidic culture platform using the focused femtosecond light, the common response, burst spikes, are generated at regular intervals along with repetitive spikes, similar to the 2D common spike pattern. The PSTH and raster plots show that the optical stimulation on a neuron in 3D environments can be reproduced.

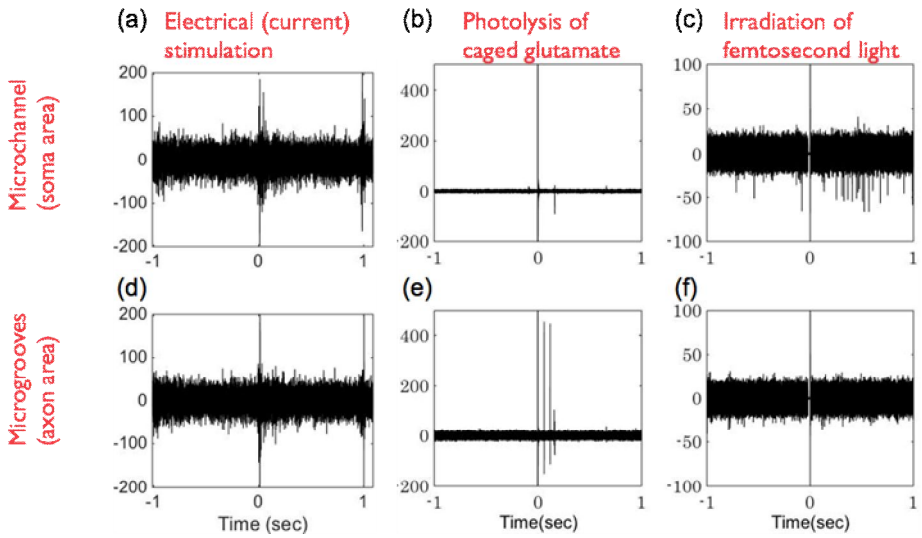

Figure 4.8. Direct comparison of the electrical stimulation, photolysis of caged glutamate, and optical stimulation by the femtosecond light. The neural response to the irradiation of the focused femtosecond light was compared with electrical stimulation and photolysis of MNI-caged glutamate. The latency of the first response time in the femtosecond light exposure is about 50 ms, slower than in the electrical stimulation and faster than in the photolysis of MNI-caged glutamate. The response to the femtosecond light emerges only from the soma, while other responses are from both the soma and the axons.

	Electrical stimulation	Photolysis of caged glutamate	Optogenetics (based on Hady AE et al. (2013)	**Irradiation of femtosecond light**
Artifact	Difficult to analyse the neural response	none	none	none
Spike Variation	broad (0 ~ 60)	0 ~10	15 ~ 30	20 ~ 30 (repetitive spikes)
Temporal resoultion	less than 1μsec	more than 20ms single pulse	40 repetition of 1sec rectangular pulse	less than 10ms single pulse (safe)
Spatial Resolution	Dependent on intervals among electrodes	367μm(diameter) at 60X (Controllable)	1.1 mm^2 at 20X (Controllable)	0.3μm at 40X lens
Latency	less than 20ms	more than 100 ms	about 50ms	about 50ms (less than 100ms)
Safe	Safe (less than 1μA)	Glutatoxicity	Possible (infection or transfection)	Safe (low intensity)
3D culture	poor spatial resolution	possible	possible	possible

Table 4.1. Summary of the response property for stimulation methods

4.3.3. Possible Mechanisms

The shapes, rate, and pattern of firing of action potentials have been reported to differ among a variety of neurons. Purkinje neurons (GABAergic projection neurons) have a spontaneous firing rate of 40 Hz, all-or-none burst spikes, and narrow shape. Their subtle differences in physiological property produce difference in the ionic conductance. To investigate the mechanism underlying the neural activation evoked by the femtosecond light, it is important to understand the firing pattern of repetitive spikes with 20–30 Hz and the spike shape of the first negative phase and the next positive phase. The distinctive properties of repetitive spiking neurons have been well studied [97]. The supra-threshold excitation of the soma evoking two or more action potentials results in repetitive spikes in the soma. It generates somatic sodium action potentials from a calcium potential generated within the soma; therefore, it was often induced by injecting long lasting depolarizing current of increasing amplitude. Interestingly, the spike shape of the femtosecond light-activated response correlates with the conclusion that the response to the femtosecond light begins from the soma.

To confirm the relationship between repetitive spikes evoked by the femtosecond light and calcium entry, we simultaneously monitored the intracellular calcium concentration in the exposed neuron, dialyzed with 100 μM Flou-4 (Life Technology, USA). Consistent with a previous observation, calcium concentration in the soma was rapidly elevated following the spikes after irradiation by the femtosecond light (Figure 4.9.).

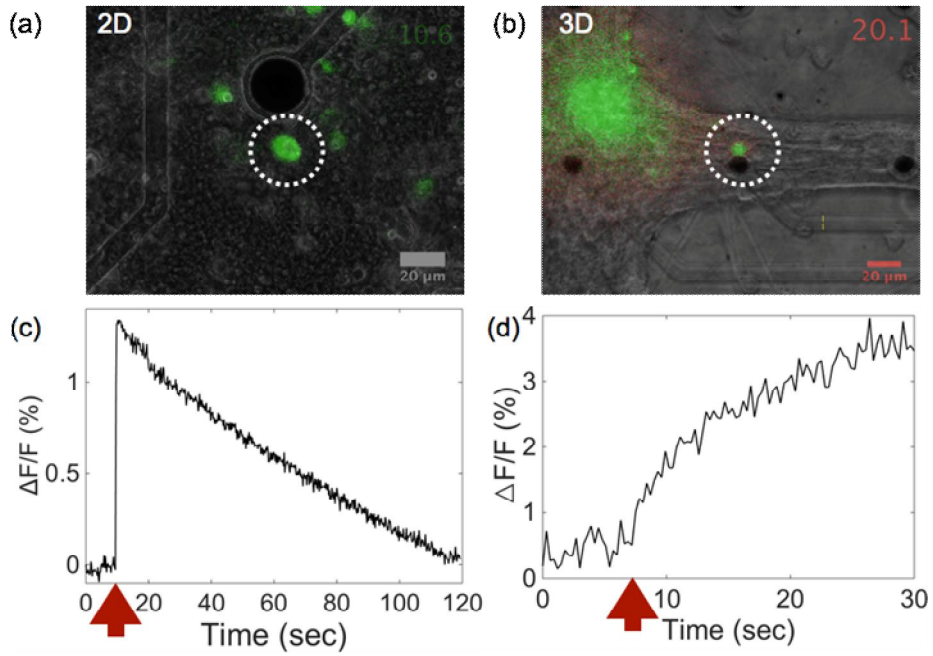

Figure 4.9. Calcium imaging using Flou-4. Calcium response to irradiation of the femtosecond light was increased. The image in 2D (a) and 3D (b) acquired at every 200ms and 300ms respectively show the increase of intracellular calcium level. The calcium level increases rapidly in 2D (c), but it increases gradually in 3D.

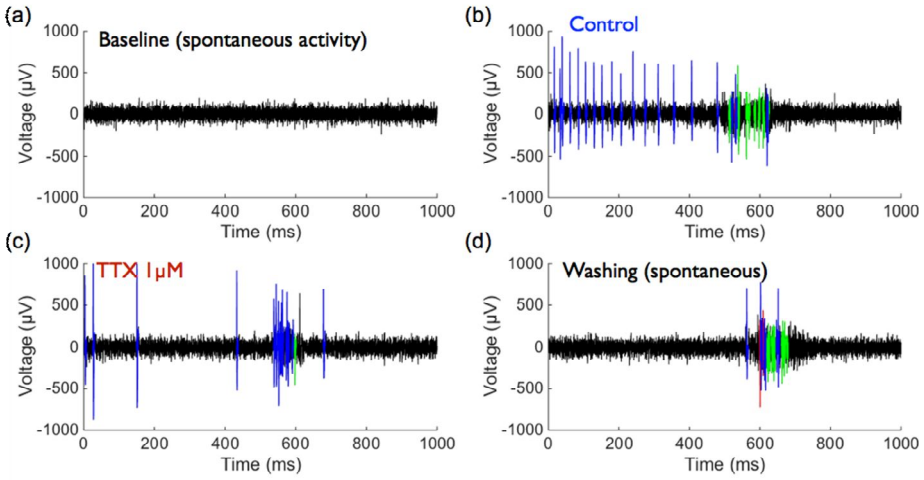

Figure 4.10. Pharmacological analysis with the voltage-sensitive Na^+ channel blocker, tetrodotoxin (TTX). Spontaneous activity without stimulation (a) and after washing (d). Neural response evoked by the focused femtosecond light (b) and with TTX treatment (c) demonstrates that the femtosecond light changes the membrane potential of the soma, opening the voltage-sensitive Na^+ channels.

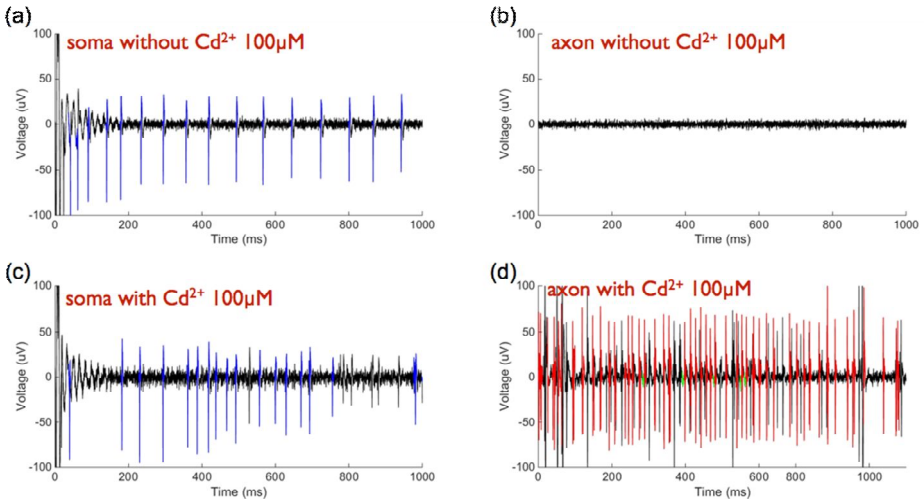

Figure 4.11. Pharmacological analysis with voltage-sensitive calcium channel blocker, cadmium chloride (Cd^{2+}). When the focused femtosecond light is delivered to the soma of the neuron, only the soma responds. However, when the neuron is treated with 100 μM Cd^{2+}, both the soma and the axons generate the repetitive spikes.

Obtaining a direct proof of the supra-threshold excitation needs other electrophysiological tools such as a voltage clamp. Instead of using other tools, we explored the voltage-dependent ion channels activated by the femtosecond light during the supra-threshold excitation of the soma as indirect proof. To complement these experiments, we treated the cells with 1 μM tetrodotoxin (TTX, abcam, USA) and 100 μM cadmium chloride (Cd^{2+}, Sigma Aldrich, USA), and measured the response to the femtosecond light (Figure 4.10, Figure 4.11). We observed that the femtosecond light generated repetitive spikes without TTX; however, TTX abolished the spiking pattern when the culture neuron was irradiated. This result showed that the TTX-sensitive sodium channels were opened by the femtosecond light, which generated the repetitive spikes. To verify the role of voltage-sensitive calcium channels opening after irradiation by the femtosecond light, cells were pre-loaded with 100 μM Cd^{2+} for 30 minutes. Cd^{2+} is a potent Ca^{2+} channel blocker and inhibits mainly voltage-sensitive Ca^{2+} channels, while the cellular uptake of Cd^{2+} occurs mainly through the Ca^{2+} channels. We examined the effect of Cd^{2+} on both soma and axon in response to the femtosecond light. The repetitive spikes changed into rapid spike trains at an irregular rate after the femtosecond light exposure. A significant alternation of the response was observed in the axons. The neural signals recorded from microgrooves in the microfluidic device showed that the action potentials of the axons appeared in response to the femtosecond light exposure after pretreatment with Cd^{2+}. We noticed that the focused femtosecond laser on the neuron evoked supra-threshold excitation of the soma, followed by

activation of the voltage-sensitive calcium channel. In addition, to determine if voltage-sensitive calcium channels inhibit the spikes, we exposed a single neuron to femtosecond light after pretreatment with 250 μM 4,4'-Diisothiocyano-2,2'-stilbenedisulfonic acid (DIDS, Sigma Aldrich, USA), a calcium-gated chloride channel blocker, for 30 min (Figure 4.14(c)). Compared with the neural response before pretreatment, the activation of the soma induced by femtosecond light did not change. However, the axonal response to the focused femtosecond light showed repetitive spikes similar to the result of pretreatment with Cd^{2+}. Furthermore, when the neuron was pretreated with the inhibitor of the calcium-activated calcium release from the calcium store for 30 minutes, the axon responded to the femtosecond light with repetitive spikes. Our data suggested that the supra-threshold excitation of the soma evoked by the femtosecond light could be involved in repetitive spikes in the soma and inhibition in the axons through calcium-activated chloride channels.

The influx of intracellular calcium is thought to have originated from the extracellular environment or intracellular calcium store. We determined precisely which source is responsible for the repetitive spikes evoked by the femtosecond light in the cultured hippocampal neurons. We used calcium-free media and added the calcium chelator EGTA (Sigma Aldrich, USA) to remove the calcium ions in the extracellular environment. However, the removal of extracellular calcium ions did not have a significant effect on the response to the femtosecond light (Figure 4.12(b)). The neuron still generated the repetitive spikes although there was low calcium ion

concentration in the extracellular environments. Therefore, we investigated the effects of the intracellular calcium store on the focused femtosecond light. We incubated the neurons with 1 μM thapsigargin (Sigma Aldrich, USA) to induce the depletion of the intracellular calcium store and bathed them with calcium free-media (DPBS-calcium free, Gibco, USA) and 100 μM EGTA. We observed that the repetitive spikes disappeared on exposure to the femtosecond light sufficient to activate the neuron (Figure 4.12(c)). Taken together, these results demonstrated that the intra-cellular calcium responsible for the repetitive spikes was released from the intracellular calcium store by the femtosecond light.

The endoplasmic reticulum (ER) and mitochondria are the major calcium storage compartments in cells. To assess the role of the ER, we used 1 μM Ryanodine (Sigma Aldrich, USA) and 50 μM 2-aminoethoxydiphenyl borate (2-APB, Sigma Aldrich, USA), blockers of the ER calcium channels. We found that the repetitive spikes disappeared, when treating with the materials and stimulating the same neuron with the light (Figure 4.13). To determine the effect of the femtosecond light on mitochondria, cyclosporine-A (Sigma Aldrich, USA) was applied to the neurons, which resulted in the inactivation of most of the responses to the femtosecond light (Figure 4.15). When comparing these data, we conclude that the femtosecond light yields the repetitive spikes through intracellular calcium increase released from the mitochondria or ER.

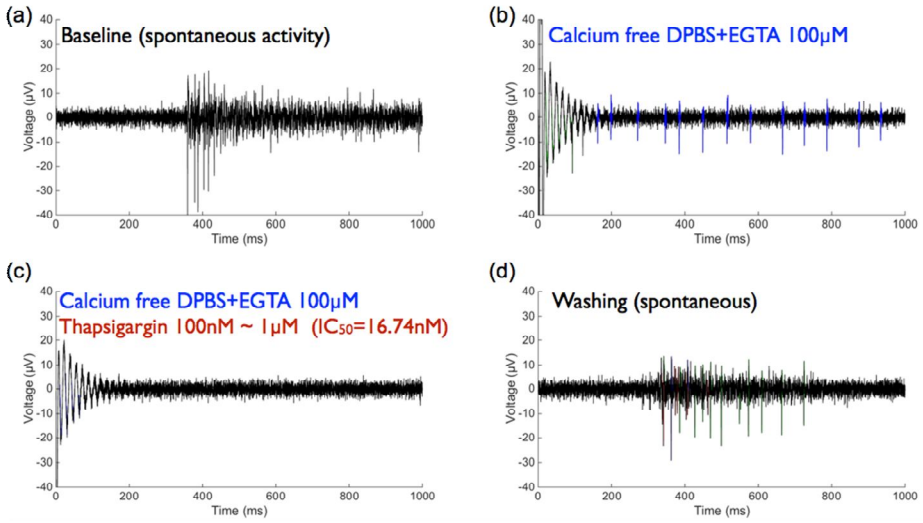

Figure 4.12. Repetitive spikes induced by the femtosecond light are involved in intracellular calcium influx from internal calcium storage. Pharmacological analysis with calcium free DPBS and 100 μM EGTA (b) shows that the extracellular calcium influx is not the main reason for the repetitive spikes evoked by the focused femtosecond light. Additionally, when the calcium ions in the intracellular calcium storages were depleted with 1 μM Thapsigargin (b), the neural response to optical stimulation disappeared.

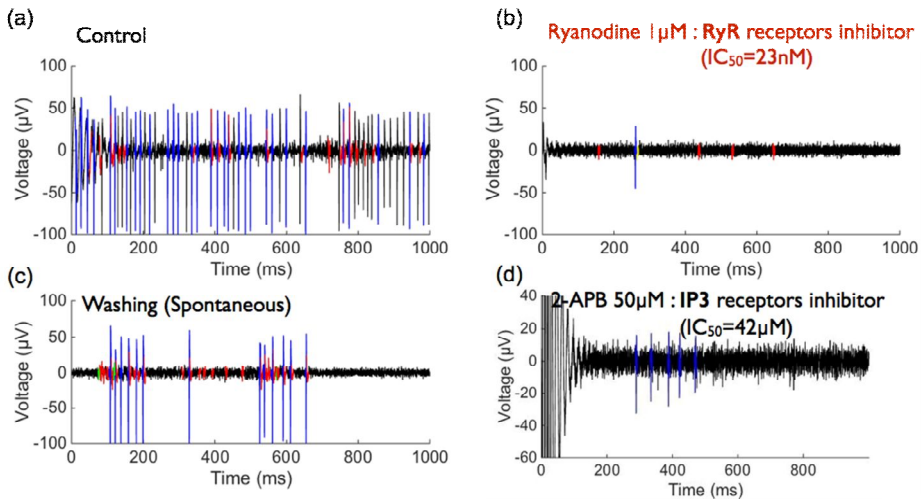

Figure 4.13. Pharmacological analysis with the ER calcium channel blocker. The results using 1 μM RyR (b) or 50 μM 2-APB (d) show that the irradiation of the focused femtosecond light evokes repetitive spikes through calcium release from the ER.

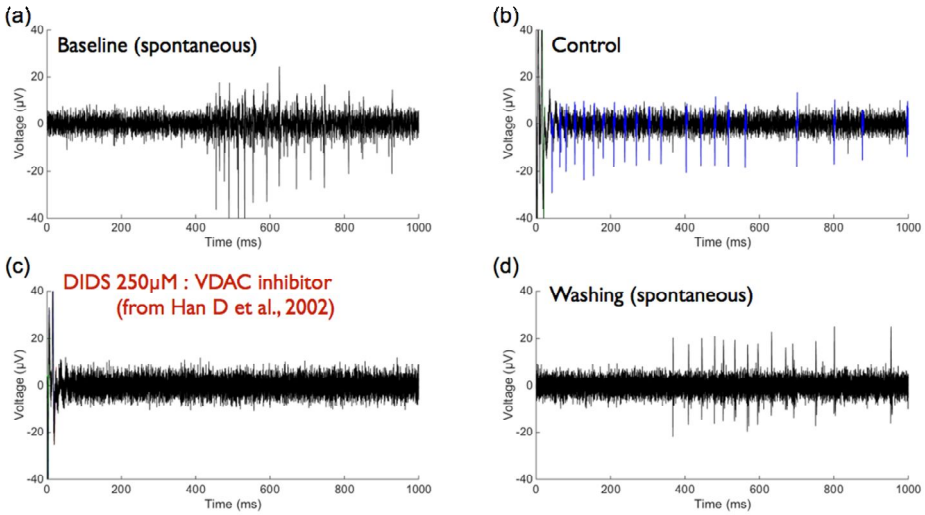

Figure 4.14. Effects of a VDAC channel blocker in the mitochondria on the repetitive spikes evoked by the femtosecond light. The pharmacological analysis with the VDAC inhibitor (250 μM DIDS) shows that the focused femtosecond light generates the repetitive spikes through calcium influx from the mitochondria

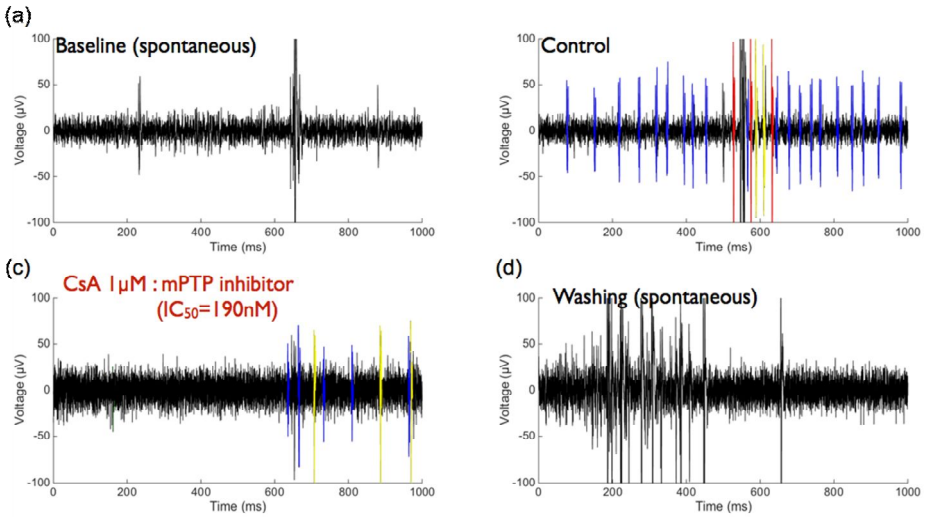

Figure 4.15. Effects of an mPTP channel blocker in the mitochondria on the repetitive spikes evoked by the femtosecond light. The pharmacological analysis with the mPTP inhibitor (1 μM cyclosporine A) shows that the focused femtosecond light generates the repetitive spikes through calcium influx from the mitochondria.

Reactive oxygen species (ROS) have been identified as targets of femtosecond-induced calcium transients. In this study, we examined whether the femtosecond light induced the repetitive spikes through ROS production. N-acetyl-cysteine (NAC, Sigma Aldrich, USA), an anti-oxidant, prevents the generation of ROS in cells. Thus, we assessed the effects of 5mM NAC treatment on irradiation by the femtosecond light. The evoked spikes are not significantly different from the repetitive spikes without NAC even though long time treatment (Figure 4.16). This result was expected, because ROS generation has been known to occur from the calcium uptake and membrane depolarization of the mitochondria, applying to turn off GFP signals [98]. However, the spike rate and pattern of the neuron pretreated with NAC showed subtle difference from the control experiment. These data suggest that the femtosecond light produces ROS in the neuron; however, it is not the main reason for generating repetitive spikes.

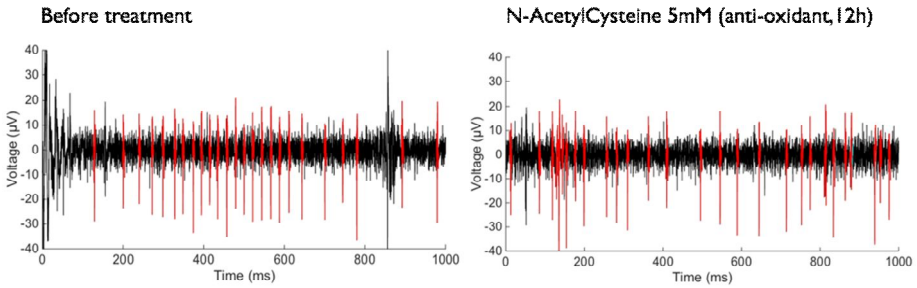

Figure 4.16. Effects of antioxidants on the repetitive spikes evoked by the femtosecond light. We explored whether the reactive oxygen species (ROS) resulted from the repetitive spikes in response to the focused femtosecond light. Pharmacological analysis with 5 mM NAC showed that the light generated the repetitive spikes without ROS.

4.4. Discussion

Despite extensive trials, implementing highly precise neural stimulation in 3D without invasiveness and external materials remains limited. Conventional techniques, like electrical stimulation, provide neural activation but with limitations. In this study, we introduce a new method to stimulate a single neuron in a 3D environment using the focused femtosecond laser. This method promises us safer and more efficient neural stimulation. The neural response to irradiation by the femtosecond light was identified as repetitive spikes at a rate of 20–30 Hz, irrespective of optical parameters such as intensity and exposure duration. Moreover, the waveform of the evoked spikes revealed that only the soma responded to irradiation by the femtosecond light. Compared to other stimulation methods, this method has the advantage of spatial and temporal resolution. Furthermore, the use of the femtosecond light is presented that it can be produced and safe.

The electrophysiological analysis of this phenomenon showed that the repetitive spikes evoked by the femtosecond light were caused by the supra-threshold excitation of the soma through intracellular calcium. Additional pharmacological experiments proved that the femtosecond light released intracellular calcium from the internal calcium stores such as the mitochondria and ER. The supra-threshold excitation of the soma was shown to be indirectly via voltage-sensitive ion channels. Moreover, we expected that the femtosecond light, reported to exhaust calcium ions in ER or mitochondria [98], would induce calcium influx from the extracellular.

However, this calcium influx from extracellular ions does pull the trigger to activate a neuron as much as from intracellular organelle.

In the case of non-neural cells [99, 100], astrocytes [95, 101, 102], and heart muscle cells [103, 104], changes were observed after two-photon intrinsic stimulation. It was reported that the two-photon intrinsic stimulation acted as a pacemaker. When isolated cardiomyocytes or small groups of cardiomyocytes were irradiated with an average power between 15 and 30 mW using an 80 fs laser with an 82 MHz repetition rate and a 780 nm center wavelength, the periodic contraction cycle was altered depending on the laser periodicity. Astrocytes were examined in succession by two teams. Both groups acquired the specimens from a primary culture of rat astrocytes, and targeted the cytosolic region rather than the membrane. One study used a laser with a 90 fs duration, 800 nm center wavelength, and 80 MHz repetition rate. The astrocytes were stimulated for 14 ms at an average power of 1560 mW. It was demonstrated that the optical stimulation induced an increase in the calcium level in the astrocytes because a transient hole was formed in the cell membrane by the femtosecond laser pulses. The other group employed a femtosecond laser providing 140 fs pulses, an 800 nm center wavelength, and an 80 MHz repetition rate. Their parameters of stimulation were 100 ms duration and an average power of 300–500 mW. The authors suggested that this phenomenon was associated with unknown molecular events, although their results were similar to those from a previous study.

	Cells	Wavelength / pulse width	Repetition rate	Duration	Power	Lens (N.A.)	Mechanism
Hirase et al. (2002)	cortical pyramidal neurons	790-850nm / 130fs	76 Mhz	30 ms	200-450 mW	x40 (0.8) x60 (0.9)	Reactive oxygen species
Hosokawa C et al. (2013)	hippocampal neurons	800 nm / 100fs	82 Mhz	15-70 ms	20-30 mW	x60 (1.0)	
Smith NI et al. (2006)	PC12	775nm / 80fs	82 Mhz	8 ms	20-80mW	x60 (0.9)	Microhole
Iwanaga S et al. (2006)	HeLa Cells	780nm / 80fs	10 kHz ~ 82Mhz	10ms ~ 100s	0.1-100mW	x60 (0.9)	Reactive oxygen species
Smith NI et al. (2008)	cardiomyocytes	780nm / 80fs	82 Mhz	8 ms	15-30 mW	x60 (0.9)	
Zhao Y et al. (2009)	astrocyte	800nm / 90fs	80Mhz	3 ms	~ 30mW	x60 (1.2)	
He H et al. (2010)	HeLa Cells	1554nm / 170fs	20Mhz	1 sec	100mW	x20 (1.0)	cytoplasm : intracellular nucleus : extracellular
Yoon JH et al. (2014)	smooth muscle cells	800nm / 120fs	80Mhz	1.96 us	700 - 1500mW	x40 (0.8)	Reactive oxygen species
Yoon JH et al. (2015)	HeLa Cells	800nm / 120fs	80Mhz	0.96 ~ 121.93 us	1W	x40 (0.8)	Laser-induced cell death
Our experiments	**hippocampal neurons**	**700 nm / 140fs**	**80Mhz**	**5~100ms**	**23-180mW**	**x60 (0.7)**	**calcium influx from intracellular ca store**

Table 4.2. Comparison with previous studies with the usage of the focused femtosecond light

The debate on how a focused femtosecond laser could activate a single neuron is currently underway. A local temperature increase is one possible mechanism for such activation. This idea is based on the first report that the infrared light induced compound action potential. Many successive studies demonstrated that the infrared light locally enhanced the membrane temperature. This temperature change may induce the opening of ion channels or changes in the capacitance value of the membrane, which depolarizes the membrane potential. The laser-induced heating was calculated based on the thermodynamic modeling and simulation using COMLSOL finite element method software [105]. With 100 mW at 800 nm, the temperature rose by 0.32 °C in the center of the laser spot and 0.17 °C at a distance 30 μm away from it. There is no doubt that this phenomenon is not involved in the optical ablation or water break down, because water break down requires a much higher energy of 200 nJ/pulse. Femtosecond pulses reduce the energy and minimize the size of the region damaged by the shock wave.

One practical consideration is the thermal risks or damaging effects from temperature increase on target and surrounding cells. However, there is no response of TRPV1 or TRPV4 channels that open when the temperature is increased in a neuron's surrounding environment. A change of 2 °C in temperature has been validated; however, modeling results show the level is below 0.5 °C when the femtosecond light is exposed to a circular area on the neurobasal media with a diameter of 2 μm. When we tried to evoke action potentials with two kinds of gold nano-rods, with maximal absorption at 780

nm and 980 nm, we did not observe any response to the femtosecond light.

In addition to this, three other hypotheses have been suggested. The first is ROS. A focused femtosecond pulsed beam is thought to generate free electrons, and subsequently, ROS by electron delivery. To explain the mechanism through ROS, there are several possibilities. One possibility is that the generation of ROS may lead to membrane depolarization through oxidative modification of the channel or ion-transport proteins. Several studies have reported that ROS have an effect on ionic channel function. One study investigated the effects of oxidative stress on several potassium channels. These channels were cloned from cardiac, brain, and T-lymphocyte cells and expressed in Xenopus oocytes. The researchers produced ROS using photo activation of Rose Bengal, a classical generator of ROS. ROS inhibited three Shaker potassium channels, one Shaw channel, and one inward rectifier potassium channel. Another possibility is that ROS may propagate and induce calcium release from the mitochondrial networks. This explanation is known as the "ROS-induced ROS release (RIRR)." The focused femtosecond pulsed laser produces ROS, and then, the ROS stimulate the cellular mitochondrial network to produce more ROS. It is a kind of positive feedback to enhance ROS production. The increased number of propagated ROS can induce intracellular calcium release. The consequence of RIRR is calcium release and a higher probability of evoked action potentials. This theory is in agreement with the first experiments using antioxidants with low-intensity and long duration irradiation. It was found that this type of irradiation was insensitive to sodium channel blocker

but sensitive to antioxidants. The depolarization in the presence of a vitamin E analog was smaller, followed by faster repolarization.

The second theory is a micro-hole in the plasma membrane. The influx of ions from outside the cells through a small hole caused by local destruction is thought to trigger action potentials. It is well known that a high-intensity laser beam can form a single, transient hole in the cell membrane. A pulsed laser was used from an 80 MHz titanium-sapphire laser with a mean power of 50–00 mW and was tightly focused using a high NA objective lens to deliver foreign DNA into cells *in vitro*. The first study on the two-photon intrinsic stimulation also demonstrated perforation at sub-femtoliter focal volumes in the cell membrane. When a brain slice was treated with TTX, the depolarized membrane potential did not disappear, but its repolarization seemed to have a fast and a slow component. However, if a microhole (or a bleb) on the neural membrane induces neural activation, the femtosecond light must always evoke repetitive spikes at any position. The experiments revealed that sequential irradiation in different positions of a neuron did not induce sequential activation.

Another hypothesis is that a calcium trigger can generate action potentials by intracellular calcium store depletion. There is no direct proof that the femtosecond light induces calcium store depletion. However, it is reported that STIM1 or CRAC channels are opened by the femtosecond light. Our result that the calcium-activated calcium release channels were opened when the femtosecond light irradiated the neuron indirectly supports the depletion of calcium stores.

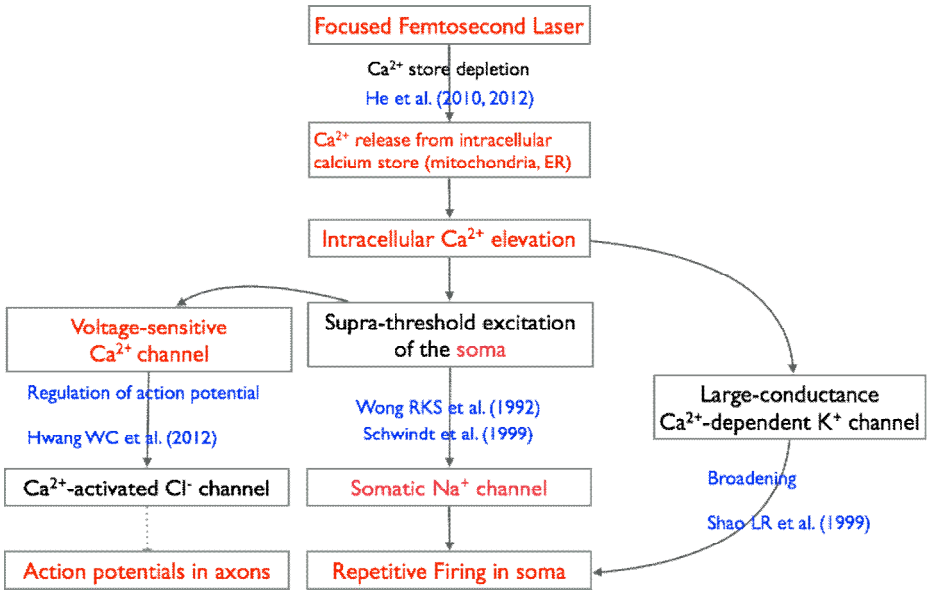

Figure 4.17. Concept diagram of possible mechanism

Chapter 5: Conclusion

Reductionism has become mainstream in modern biology over the past century. The individual particles of a cellular organism influence cellular function and structure. Therefore, the control in most experiments requires well-defined spatial or temporal resolution. In neuroscience, acutely spatial or temporal stimulation is important to investigate several aspects such as synaptic connectivity, neural circuit mapping, and single neuron dynamics. Compared to conventional electrophysiology such as the patch clamp, more knowledge can be acquired regarding dendritic spines and synapses if they were stimulated under conditions just sufficient to evoke a response from a single unit. From this perspective, photo-stimulation can provide scientists a unique and powerful means of interacting with cellular physiology. Because light passes through cell membranes, photo-stimulation can rapidly affect cellular compartments in an intracellular or extracellular approach when its delivered energy is sufficient. Moreover, optical stimulation can replace electrical stimulation. Optical stimulation is advantageous as a non-contact method, while electrical current is delivered via direct contact through electrodes. Optical stimulation also avoids the production of artifact responses that occur with electrical stimulation at the stimulating and recording electrodes. In addition, optical stimulation can be accomplished with higher spatial selectivity than electrical current, as we mentioned previously.

Compared to the other optical simulation methods, the femtosecond stimulation is able to offer a new tool for the extensive fields of neuroscience and neural engineering. Photochemical molecules such as caged glutamate or optogenetics have limitations of slower response timing even with their high spatial and temporal resolution. Most of them were used to identify neural circuits or define their connection, because the late response time was not crucial in such studies. However, the early response with precise spike timing analysis is a prerequisite for functional connectivity to quantify the brain connectivity or neural process in the brain and encode (decode) the real information in (from) spike trains. Therefore, the photochemical molecules have narrower applications than conventional electrical stimulation. However, the neural stimulation with the focused femtosecond laser can be used in fields where electrical stimulation is being used. Besides, it allows high spatial resolution to observe even the synapse area.

Technological and methodological advances in optical stimulation will result in new possibilities in *in-vivo* experiments. In order to deliver photons into the brain, an implanted optical fiber should be developed, extending from a light source through the skull and into the targeted brain regions. However, the optical fiber also is vulnerable to damage caused by movement of the animal, and its implantation may result in tissue damage in the brain. Moreover, the femtosecond light will experience dispersion and power attenuation when passing through the optical fiber. Therefore, new kinds of optic fibers are required to overcome these drawbacks and to deliver the femtosecond light successfully for *in vivo* application.

Our results allow further studies using a new brain stimulation technique without the need for external materials for in vivo application. Together, the high level of spatiotemporal resolution, coupled with the ability to regulate specific populations of neurons, offers a unique advantage compared with more traditional approaches to neuro-modulation. Additionally, based on the placement of the implanted cranial optical fiber, researchers can manipulate only the postsynaptic, presynaptic, and/or axonal membrane.

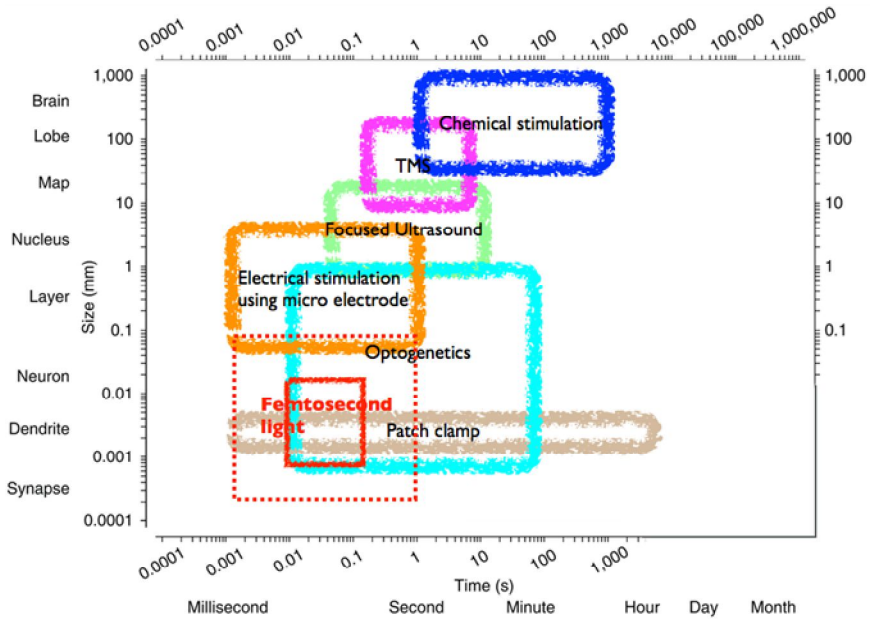

Figure 5.1. Comparison of various neural stimulation methods in the view of spatial and temporal resolution

Bibliography

[1] Piccolino M. Luigi Galvani and animal electricity: two centuries after the foundation of electrophysiology. Trends Neurosci 1997;20:443-8.

[2] Renshaw B, Forbes A, Morison BR. Activity of isocortex and hippocampus: Electrical studies with micro-electrodes. J Neurophysiol 1940;3:74-105.

[3] Hubel DH, Wiesel TN. Receptive fields of single neurones in the cat's striate cortex. J Physiol 1959;148:574-91.

[4] Mountcastle VB. Modality and topographic properties of single neurons of cat's somatic sensory cortex. J Neurophysiol 1957;20:408-34.

[5] Phillips CG. Intracellular records from Betz cells in the cat. Q J Exp Physiol Cogn Med Sci 1956;41:58-69.

[6] Coombs JS, Curtis DR, Eccles JC. The electrical constants of the motoneurone membrane. J Physiol 1959;145:505-28.

[7] Coombs JS, Eccles JC, Fatt P. The electrical properties of the motoneurone membrane. J Physiol 1955;130:291-325.

[8] Eccles JC. Membrane time constants of cat motoneurons and time courses of synptic action. Exp Neurol 1961;4:1-22.

[9] Kandel ER, Spencer WA. Excitation and inhibition of single pyramidal cells during hippocampal seizure. Exp Neurol 1961;4:162-79.

[10] Nelson PG, Lux HD. Some electrical measurements of motoneuron parameters. Biophys J 1970;10:55-73.

[11] Gray CM, Maldonado PE, Wilson M, McNaughton B. Tetrodes markedly improve the reliability and yield of multiple single-unit isolation from multi-unit recordings in cat striate cortex. J Neurosci Methods 1995;63:43-54.

[12] Thomas CA, Jr., Springer PA, Loeb GE, Berwald-Netter Y, Okun LM. A miniature microelectrode array to monitor the bioelectric activity of cultured cells. Exp Cell Res 1972;74:61-6.
[13] Charles AC, Merrill JE, Dirksen ER, Sanderson MJ. Intercellular signaling in glial cells: calcium waves and oscillations in response to mechanical stimulation and glutamate. Neuron 1991;6:983-92.
[14] Ahn DK, Lim EJ, Kim BC, Yang GY, Lee MK, Ju JS, et al. Compression of the trigeminal ganglion produces prolonged nociceptive behavior in rats. Eur J Pain 2009;13:568-75.
[15] Kobayashi S, Baba H, Uchida K, Kokubo Y, Kubota C, Yamada S, et al. Effect of mechanical compression on the lumbar nerve root: localization and changes of intraradicular inflammatory cytokines, nitric oxide, and cyclooxygenase. Spine (Phila Pa 1976) 2005;30:1699-705.
[16] Song XJ, Hu SJ, Greenquist KW, Zhang JM, LaMotte RH. Mechanical and thermal hyperalgesia and ectopic neuronal discharge after chronic compression of dorsal root ganglia. J Neurophysiol 1999;82:3347-58.
[17] Lulevich V, Zink T, Chen HY, Liu FT, Liu GY. Cell mechanics using atomic force microscopy-based single-cell compression. Langmuir 2006;22:8151-5.
[18] Bernick KB, Prevost TP, Suresh S, Socrate S. Biomechanics of single cortical neurons. Acta Biomater 2011;7:1210-9.
[19] Lu YB, Franze K, Seifert G, Steinhauser C, Kirchhoff F, Wolburg H, et al. Viscoelastic properties of individual glial cells and neurons in the CNS. Proc Natl Acad Sci U S A 2006;103:17759-64.
[20] Papadopoulou EL, Samara A, Barberoglou M, Manousaki A, Pagakis SN, Anastasiadou E, et al. Silicon scaffolds promoting three-dimensional neuronal web of cytoplasmic processes. Tissue Eng Part C Methods 2010;16:497-502.
[21] Pautot S, Wyart C, Isacoff EY. Colloid-guided assembly of oriented 3D neuronal networks. Nat Methods 2008;5:735-40.

[22] Tang-Schomer MD, White JD, Tien LW, Schmitt LI, Valentin TM, Graziano DJ, et al. Bioengineered functional brain-like cortical tissue. Proc Natl Acad Sci U S A 2014;111:13811-6.
[23] Yang F, Murugan R, Wang S, Ramakrishna S. Electrospinning of nano/micro scale poly(L-lactic acid) aligned fibers and their potential in neural tissue engineering. Biomaterials 2005;26:2603-10.
[24] Kim S, Lee H, Chung M, Jeon NL. Engineering of functional, perfusable 3D microvascular networks on a chip. Lab Chip 2013;13:1489-500.
[25] Sung JH, Yu J, Luo D, Shuler ML, March JC. Microscale 3-D hydrogel scaffold for biomimetic gastrointestinal (GI) tract model. Lab Chip 2011;11:389-92.
[26] Huh D, Hamilton GA, Ingber DE. From 3D cell culture to organs-on-chips. Trends Cell Biol 2011;21:745-54.
[27] Yamada M, Utoh R, Ohashi K, Tatsumi K, Yamato M, Okano T, et al. Controlled formation of heterotypic hepatic micro-organoids in anisotropic hydrogel microfibers for long-term preservation of liver-specific functions. Biomaterials 2012;33:8304-15.
[28] Farber IC, Grinvald A. Identification of presynaptic neurons by laser photostimulation. Science 1983;222:1025-7.
[29] Gumera C, Rauck B, Wang YD. Materials for central nervous system regeneration: bioactive cues. J Mater Chem 2011;21:7033-51.
[30] Augustine GJ. Illuminating the location of brain glutamate receptors. Nat Neurosci 2001;4:1051-2.
[31] Pettit DL, Wang SS, Gee KR, Augustine GJ. Chemical two-photon uncaging: a novel approach to mapping glutamate receptors. Neuron 1997;19:465-71.
[32] Nikolenko V, Poskanzer KE, Yuste R. Two-photon photostimulation and imaging of neural circuits. Nat Methods 2007;4:943-50.

[33] Matsuzaki M, Ellis-Davies GCR, Nemoto T, Miyashita Y, Iino M, Kasai H. Dendritic spine geometry is critical for AMPA receptor expression in hippocampal CA1 pyramidal neurons. Nature Neuroscience 2001;4:1086-92.
[34] Arenkiel BR, Peca J, Davison IG, Feliciano C, Deisseroth K, Augustine GJ, et al. In vivo light-induced activation of neural circuitry in transgenic mice expressing channelrhodopsin-2. Neuron 2007;54:205-18.
[35] Carroll EC, Berlin S, Levitz J, Kienzler MA, Yuan Z, Madsen D, et al. Two-photon brightness of azobenzene photoswitches designed for glutamate receptor optogenetics. Proc Natl Acad Sci U S A 2015;112:E776-85.
[36] Kruman II, Culmsee C, Chan SL, Kruman Y, Guo ZH, Penix L, et al. Homocysteine elicits a DNA damage response in neurons that promotes apoptosis and hypersensitivity to excitotoxicity. J Neurosci 2000;20:6920-6.
[37] Doble A. The role of excitotoxicity in neurodegenerative disease: Implications for therapy. Pharmacol Therapeut 1999;81:163-221.
[38] Budd SL, Nicholls DG. Mitochondria, calcium regulation, and acute glutamate excitotoxicity in cultured cerebellar granule cells. J Neurochem 1996;67:2282-91.
[39] Arundine M, Tymianski M. Molecular mechanisms of calcium-dependent neurodegeneration in excitotoxicity. Cell Calcium 2003;34:325-37.
[40] Oron D, Papagiakoumou E, Anselmi F, Emiliani V. Two-photon optogenetics. Prog Brain Res 2012;196:119-43.
[41] Gunaydin LA, Yizhar O, Berndt A, Sohal VS, Deisseroth K, Hegemann P. Ultrafast optogenetic control. Nat Neurosci 2010;13:387-92.
[42] Fenno L, Yizhar O, Deisseroth K. The development and application of optogenetics. Annu Rev Neurosci 2011;34:389-412.
[43] Tye KM, Deisseroth K. Optogenetic investigation of neural circuits underlying brain disease in animal models. Nat Rev Neurosci 2012;13:251-66.

[44] Gavrilov LR, Tsirulnikov EM, Davies IA. Application of focused ultrasound for the stimulation of neural structures. Ultrasound Med Biol 1996;22:179-92.
[45] Bachtold MR, Rinaldi PC, Jones JP, Reines F, Price LR. Focused ultrasound modifications of neural circuit activity in a mammalian brain. Ultrasound Med Biol 1998;24:557-65.
[46] Yoo SS, Bystritsky A, Lee JH, Zhang YZ, Fischer K, Min BK, et al. Focused ultrasound modulates region-specific brain activity. Neuroimage 2011;56:1267-75.
[47] Menz MD, Oralkan O, Khuri-Yakub PT, Baccus SA. Precise Neural Stimulation in the Retina Using Focused Ultrasound. J Neurosci 2013;33:4550-+.
[48] Tyler WJ, Tufail Y, Finsterwald M, Tauchmann ML, Olson EJ, Majestic C. Remote Excitation of Neuronal Circuits Using Low-Intensity, Low-Frequency Ultrasound. Plos One 2008;3.
[49] White PJ, Clement GT, Hynynen K. Longitudinal and shear mode ultrasound propagation in human skull bone. Ultrasound Med Biol 2006;32:1085-96.
[50] Clement GT, White PJ, King RL, McDannold N, Hynynen K. A magnetic resonance imaging-compatible, large-scale array for trans-skull ultrasound surgery and therapy. J Ultrasound Med 2005;24:1117-25.
[51] Fry WJ, Wulff VJ, Tucker D, Fry FJ. Physical Factors Involved in Ultrasonically Induced Changes in Living Systems .1. Identification of Non-Temperature Effects. J Acoust Soc Am 1950;22:867-76.
[52] Fry WJ, Tucker D, Fry FJ, Wulff VJ. Physical Factors Involved in Ultrasonically Induced Changes in Living Systems - .2. Amplitude Duration Relations and the Effect of Hydrostatic Pressure for Nerve Tissue. J Acoust Soc Am 1951;23:364-8.

[53] Gavrilov LR, Tsirulnikov EM, Davies IAI. Application of focused ultrasound for the stimulation of neural structures. Ultrasound in Medicine and Biology 1996;22:179-92.
[54] Tufail Y, Matyushov A, Baldwin N, Tauchmann ML, Georges J, Yoshihiro A, et al. Transcranial Pulsed Ultrasound Stimulates Intact Brain Circuits. Neuron 2010;66:681-94.
[55] Kim H, Chiu A, Lee SD, Fischer K, Yon SS. Focused Ultrasound-mediated Non-invasive Brain Stimulation: Examination of Sonication Parameters. Brain Stimul 2014;7:748-56.
[56] Chen R, Classen J, Gerloff C, Celnik P, Wassermann EM, Hallett M, et al. Depression of motor cortex excitability by low-frequency transcranial magnetic stimulation. Neurology 1997;48:1398-403.
[57] Ilmoniemi RJ, Virtanen J, Ruohonen J, Karhu J, Aronen HJ, Naatanen R, et al. Neuronal responses to magnetic stimulation reveal cortical reactivity and connectivity. Neuroreport 1997;8:3537-40.
[58] Pascual-Leone A, Walsh V, Rothwell J. Transcranial magnetic stimulation in cognitive neuroscience--virtual lesion, chronometry, and functional connectivity. Curr Opin Neurobiol 2000;10:232-7.
[59] Walsh V, Cowey A. Transcranial magnetic stimulation and cognitive neuroscience. Nat Rev Neurosci 2000;1:73-9.
[60] Calvo-Merino B, Haggard P. [Transcranial magnetic stimulation. Applications in cognitive neuroscience]. Rev Neurol 2004;38:374-80.
[61] Abler B, Walter H, Wunderlich A, Grothe J, Schonfeldt-Lecuona C, Spitzer M, et al. Side effects of transcranial magnetic stimulation biased task performance in a cognitive neuroscience study. Brain Topogr 2005;17:193-6.
[62] Sandrini M, Umilta C, Rusconi E. The use of transcranial magnetic stimulation in cognitive neuroscience: a new synthesis of methodological issues. Neurosci Biobehav Rev 2011;35:516-36.
[63] Barker AT, Jalinous R. Non-Invasive Magnetic Stimulation of Human Motor Cortex. Lancet 1985;1:1106-7.

[64] Lewicki MS. A review of methods for spike sorting: the detection and classification of neural action potentials. Network-Comp Neural 1998;9:R53-R78.
[65] Pillow JW, Shlens J, Chichilnisky EJ, Simoncelli EP. A Model-Based Spike Sorting Algorithm for Removing Correlation Artifacts in Multi-Neuron Recordings. Plos One 2013;8.
[66] Calabrese A, Paninski L. Kalman filter mixture model for spike sorting of non-stationary data. J Neurosci Meth 2011;196:159-69.
[67] Hosmane S, Fournier A, Wright R, Rajbhandari L, Siddique R, Yang IH, et al. Valve-based microfluidic compression platform: single axon injury and regrowth. Lab on a chip 2011;11:3888-95.
[68] Callaway EM, Yuste R. Stimulating neurons with light. Current Opinion in Neurobiology 2002;12:587-92.
[69] Katz LC. Local Circuitry of Identified Projection Neurons in Cat Visual-Cortex Brain-Slices. J Neurosci 1987;7:1223-49.
[70] Dalva MB, Katz LC. Rearrangements of Synaptic Connections in Visual-Cortex Revealed by Laser Photostimulation (Vol 265, Pg 255, 1994). Science 1994;265:1644-.
[71] Dantzker JL, Callaway EM. Laminar sources of synaptic input to cortical inhibitory interneurons and pyramidal neurons. Nature Neuroscience 2000;3:701-7.
[72] Sawatari A, Callaway EM. Diversity and cell type specificity of local excitatory connections to neurons in layer 3B of monkey primary visual cortex. Neuron 2000;25:459-71.
[73] Yabuta NH, Sawatari A, Callaway EM. Two functional channels from primary visual cortex to dorsal visual cortical areas. Science 2001;292:297-300.
[74] Callaway EM. Cell type specificity of local cortical connections. J Neurocytol 2002;31:231-7.

[75] Lee CC, Sherman SM. Modulator property of the intrinsic cortical projection from layer 6 to layer 4. Front Syst Neurosci 2009;3:3.
[76] Shepherd GMG, Pologruto TA, Svoboda K. Circuit analysis of experience-dependent plasticity in the developing rat barrel cortex. Neuron 2003;38:277-89.
[77] Schubert D, Staiger JF, Cho N, Kotter R, Zilles K, Luhmann HJ. Layer-specific intracolumnar and transcolumnar functional connectivity of layer V pyramidal cells in rat barrel cortex. J Neurosci 2001;21:3580-92.
[78] Schubert D, Kotter R, Staiger JF. Mapping functional connectivity in barrel-related columns reveals layer- and cell type-specific microcircuits. Brain Struct Funct 2007;212:107-19.
[79] Shepherd GMG, Svoboda K. Laminar and columnar organization of ascending excitatory projections to layer 2/3 pyramidal neurons in rat barrel cortex. J Neurosci 2005;25:5670-9.
[80] Briggs F, Callaway EM. Layer-specific input to distinct cell types in layer 6 of monkey primary visual cortex. J Neurosci 2001;21:3600-8.
[81] Yoshimura Y, Dantzker JLM, Callaway EM. Excitatory cortical neurons form fine-scale functional networks. Nature 2005;433:868-73.
[82] Shepherd GMG, Stepanyants A, Bureau I, Chklovskii D, Svoboda K. Geometric and functional organization of cortical circuits. Nature Neuroscience 2005;8:782-90.
[83] Schubert D, Kotter R, Zilles K, Luhmann HJ, Staiger JF. Cell type-specific circuits of cortical layer IV spiny neurons. J Neurosci 2003;23:2961-70.
[84] Katz LC, Shatz CJ. Synaptic activity and the construction of cortical circuits. Science 1996;274:1133-8.
[85] Roerig B, Nelson DA, Katz LC. Fast synaptic signaling by nicotinic acetylcholine and serotonin 5-HT3 receptors in developing visual cortex. J Neurosci 1997;17:8353-62.

[86] Kandler K, Katz LC, Kauer JA. Focal photolysis of caged glutamate produces long-term depression of hippocampal glutamate receptors. Nature Neuroscience 1998;1:119-23.
[87] Dodt HU, Eder M, Frick A, Zieglgansberger W. Precisely localized LTD in the neocortex revealed by infrared-guided laser stimulation. Science 1999;286:110-3.
[88] Shi SH, Hayashi Y, Petralia RS, Zaman SH, Wenthold RJ, Svoboda K, et al. Rapid spine delivery and redistribution of AMPA receptors after synaptic NMDA receptor activation. Science 1999;284:1811-6.
[89] Matsuzaki M, Honkura N, Ellis-Davies GCR, Kasai H. Structural basis of long-term potentiation in single dendritic spines. Nature 2004;429:761-6.
[90] Furuta T, Wang SSH, Dantzker JL, Dore TM, Bybee WJ, Callaway EM, et al. Brominated 7-hydroxycoumarin-4-ylmethyls: Photolabile protecting groups with biologically useful cross-sections for two photon photolysis. P Natl Acad Sci USA 1999;96:1193-200.
[91] Pettit DL, Wang SSH, Gee KR, Augustine GJ. Chemical two-photon uncaging: a novel approach to mapping glutamate receptors. Neuron 1997;19:465-71.
[92] Allegre G, Avrillier S, Albefessard D. Stimulation in the Rat of a Nerve-Fiber Bundle by a Short Uv Pulse from an Excimer-Laser. Neurosci Lett 1994;180:261-4.
[93] Uzdensky AB, Savransky VV. Single neuron response to pulse-periodic laser microirradiation. Action spectra and two-photon effect. J Photoch Photobio B 1997;39:224-8.
[94] Hirase H, Nikolenko V, Goldberg JH, Yuste R. Multiphoton stimulation of neurons. J Neurobiol 2002;51:237-47.
[95] Zhao YA, Liu XL, Zhou W, Zeng SQ. Astrocyte-to-neuron signaling in response to photostimulation with a femtosecond laser. Appl Phys Lett 2010;97.

[96] Hosokawa C, Sakamoto Y, Kudoh SN, Hosokawa Y, Taguchi T. Femtosecond laser-induced stimulation of a single neuron in a neuronal network. Appl Phys a-Mater 2013;110:607-12.
[97] Brumberg JC, Nowak LG, McCormick DA. Ionic mechanisms underlying repetitive high-frequency burst firing in supragranular cortical neurons. J Neurosci 2000;20:4829-43.
[98] He H, Li SY, Wang SY, Hu ML, Cao YJ, Wang CY. Manipulation of cellular light from green fluorescent protein by a femtosecond laser. Nat Photonics 2012;6:651-6.
[99] He H, Wang SY, Li X, Li SY, Hu ML, Cao YJ, et al. Ca2+ waves across gaps in non-excitable cells induced by femtosecond laser exposure. Appl Phys Lett 2012;100.
[100] Yoon J, Ryu SW, Lee S, Choi C. Cytosolic Irradiation of Femtosecond Laser Induces Mitochondria-dependent Apoptosis-like Cell Death via Intrinsic Reactive Oxygen Cascades. Sci Rep-Uk 2015;5.
[101] Choi M, Yoon J, Ku T, Choi K, Choi C. Label-free optical activation of astrocyte in vivo. J Biomed Opt 2011;16.
[102] Zhao Y, Zhang Y, Liu XL, Lv XH, Zhou W, Luo QM, et al. Photostimulation of astrocytes with femtosecond laser pulses. Opt Express 2009;17:1291-8.
[103] Yoon J, Choi M, Ku T, Choi WJ, Choi C. Optical induction of muscle contraction at the tissue scale through intrinsic cellular amplifiers. J Biophotonics 2014;7:597-606.
[104] Smith NI, Kumamoto Y, Iwanaga S, Ando J, Fujita K, Kawata S. A femtosecond laser pacemaker for heart muscle cells. Opt Express 2008;16:8604-16.
[105] Ebbesen CL, Bruus H. Analysis of laser-induced heating in optical neuronal guidance. J Neurosci Methods 2012;209:168-77.

초 록

뇌를 포함한 신경계를 구성하는 신경세포는 전기적 방법과 화학적 방법을 이용해 생체내 정보를 전달하고 처리한다. 이런 신경세포를 조절하는 주요한 방법은 전극을 통해 전류나 전압차를 신경세포에 주는 전기적 자극 방법이다. 하지만, 이런 전기적 자극 방법은 침습성, 낮은 공간분해능, 또한 과전압(또는 과전류)로 인한 세포 파괴등의 한계를 갖고 있다. 그래서 본 연구에서는, 신경세포를 자극하는 새로운 방법으로, 펨토초 빛을 이용해 신경세포를 활성화하는 방법을 제시하고 가능한 기작에 대해 토의하려고 한다.

주요한 연구방법으로, 평판형 미세전극배열과 미세유체 플랫폼을 결합하여, 펨토초 빛에 대한 신경 세포의 세포체와 축삭의 반응을 관찰하였다. 또한, 신경세포를 현미경 위에서 살아있는 상태로 자극하고 그 반응을 관찰하기 위해 주문제작한 라이브셀

챔버를 사용하였다. 뿐만아니라, 펨토초 빛에 반응해 발생한 신호를 신경 신호 분류 방법을 이용해 분석하였다.

펨토초 빛을 이용해 신경세포를 자극했을 때, 신경 세포의 반응은 연속적이고 불규칙적으로 나온다. 또한, 신경 세포의 세포체를 자극했을 때만, 신경세포는 펨토초 빛에 대해 반응을 보인다. 뿐만아니라, 펨토초 빛에 대한 신경 세포의 반응은 전기적인 자극 방법이나 신경전달 물질의 광분해를 이용한 분비 방법과 전혀 다르다.

펨토초 빛에 반응에서 신경세포의 세포체에 발생하는 반복적인 스파이크가 세포체내 역치값 이상의 활성으로 발화됨을 확인하였다. 이런 활성으로, 전압의존적인 나트륨이온 채널과 칼슘이온 채널이 열린다. 뿐만이나라, 칼슘이온채널이 열리기 때문에 펨토초에 대한 신경세포의 반응은 세포체에서만 나타남을 확인했다. 이 때, 세포내부에 유입되는 칼슘이온은 세포 내부 칼슘이온 저장소인, ER과 미토콘드리아에서 나오는 것으로

확인되었다. 하지만, 기존에 알려져있던 ROS나 온도 효과는 주된 영향은 아니나 미미하게 영향을 미치고 있음을 확인하였다.

본 연구 결과를 확장해 생체내 환경에 실험을 할 수 있다면, 새로운 자극방법및 치료기기로 사용할 수 있을 것이다.

주요어: 펨토초 빛, 신경세포, 광자극, 평판형 미세전극, 칼슘이온농도 증가

학 번: 2011 -30132